

การปลูกฟิล์มบางเอนกประสงค์เซอร์โคเนียมไนไตรด์โดยวิธีไอเอทีพีดีซีแมกนีตรอนสเป็คเตอริง



นางสาวจิรวรรณ แสนทน

# ศูนย์วิจัยทรัพยากร จุฬาลงกรณ์มหาวิทยาลัย

วิทยานิพนธ์นี้เป็นส่วนหนึ่งของการศึกษาตามหลักสูตรปริญญาวิทยาศาสตรมหาบัณฑิต

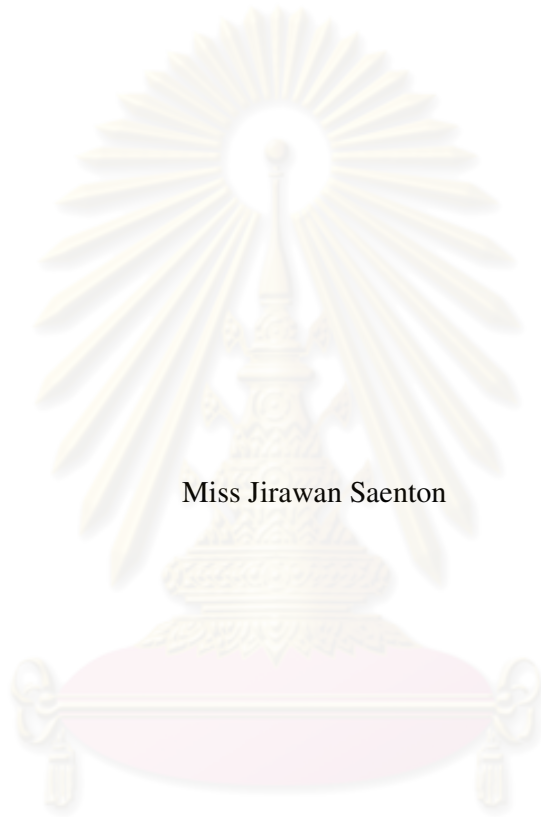
สาขาวิชาฟิสิกส์ ภาควิชาฟิสิกส์

คณะวิทยาศาสตร์ จุฬาลงกรณ์มหาวิทยาลัย

ปีการศึกษา 2552

ลิขสิทธิ์ของจุฬาลงกรณ์มหาวิทยาลัย

GROWTH OF MULTIFUNCTIONAL ZIRCONIUM NITRIDE THIN FILMS BY  
REACTIVE DC MAGNETRON SPUTTERING



Miss Jirawan Saenton

ศูนย์วิทยทรัพยากร  
จุฬาลงกรณ์มหาวิทยาลัย  
A Thesis Submitted in Partial Fulfillment of the Requirements  
for the Degree of Master of Science Program in Physics

Department of Physics

Faculty of Science

Chulalongkorn University

Academic Year 2009

Copyright of Chulalongkorn University

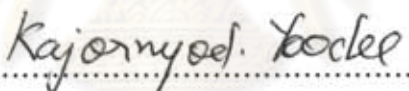
Thesis Title           GROWTH OF MULTIFUNCTIONAL ZIRCONIUM  
                                  NITRIDE THIN FILMS BY REACTIVE DC MAGNETRON  
                                  SPUTTERING  
By                         Miss Jirawan Saenton  
Field of Study         Physics  
Thesis Advisor        Assistant Professor Sukkaneste Tungasmita, Ph.D.  
Thesis Co-Advisor   Assistant Professor Sakuntam Sanorpim, Ph.D.

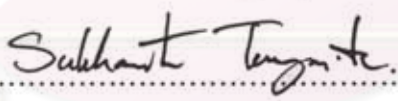
---

Accepted by the Faculty of Science, Chulalongkorn University in Partial  
Fulfillment of the Requirements for the Master's Degree

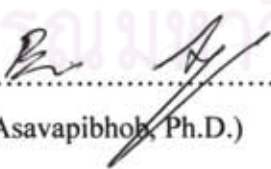
  
.....Dean of the Faculty of Science  
(Professor Supot Hannongbua, Dr.rer.nat.)

THESIS COMMITTEE

  
..... Chairman  
(Assistant Professor Kajornyod Yoodee, Ph.D.)

  
..... Thesis Advisor  
(Assistant Professor Sukkaneste Tungasmita, Ph.D.)

  
.....Thesis Co- Advisor  
(Assistant Professor Sakuntam Sanorpim, Ph.D.)

  
..... Examiner  
(Burin Asavapibhob, Ph.D.)

  
.....External Examiner  
(Associate Professor Surasing Chaiyakun, Ph.D.)

จิรวรรณ แสนทน: การปลูกฟิล์มบางเอนกประสงค์เซอร์โคเนียมไนไตรด์โดยวิธีรีแอกทีฟดีซีแมกนีตรอนสปัตเตอร์ริง. (GROWTH OF MULTIFUNCTIONAL ZIRCONIUM NITRIDE THIN FILMS BY REACTIVE DC MAGNETRON SPUTTERING)  
 อ.ที่ปรึกษาวิทยานิพนธ์หลัก: ผศ.ดร. สุกคเณศ ดุงคะสมิต, อ.ที่ปรึกษาวิทยานิพนธ์ร่วม: ผศ.ดร. สกฤทธรม เสนาะพิมพ์, 57 หน้า.

ฟิล์มบางเซอร์โคเนียมไนไตรด์ปลูกลงบนวัสดุรองรับซิลิกอนระนาบ(100) โดยวิธีรีแอกทีฟดีซีแมกนีตรอนสปัตเตอร์ริง ที่ความดันย่อยของแก๊สไนโตรเจนต่างกัน และการระดมยิงไอออนซึ่งมีพลังงานต่างกันระหว่างการปลูกฟิล์มโดยไบอัสโวลต์เทจ สำหรับสภาวะที่เหมาะสม ฟิล์มเซอร์โคเนียมไนไตรด์ปลูกที่ความดันย่อยแก๊สไนโตรเจนระหว่าง 14-17% ของความดันรวม แสดงองค์ประกอบทางเคมีที่เหมาะสมซึ่งฟิล์มมีสีทอง เราพบว่าความดันย่อยของแก๊สไนโตรเจนมีผลอย่างมากต่อ ธาตุองค์ประกอบของวัสดุ อัตราการปลูกฟิล์ม ทิศทางของผลึก และสีของฟิล์ม การเปลี่ยนแปลงพลังงานของไอออนอยู่ระหว่าง 8 ถึง 108 อิเล็กตรอนโวลต์ พลังงานของไอออนมีผลเพียงเล็กน้อยต่อองค์ประกอบทางเคมีที่เหมาะสม แต่สามารถช่วยเพิ่มความแข็งและลดความขรุขระของผิวเซอร์โคเนียมไนไตรด์ระนาบ (111) เป็นระนาบที่เด่น สำหรับทุกเงื่อนไขการปลูกฟิล์ม ค่าความแข็งที่มากที่สุดของฟิล์มบางเซอร์โคเนียมไนไตรด์คือ 38.7 จิกะปาสคาล ซึ่งได้จากการปลูกฟิล์ม เมื่อใช้พลังงานไอออนที่ 38 อิเล็กตรอนโวลต์ หลังจากการอบฟิล์มเซอร์โคเนียมไนไตรด์ องค์ประกอบทางเคมีของฟิล์มมีการเปลี่ยนแปลงเล็กน้อย แต่สีของฟิล์มไม่เปลี่ยน ผลดังกล่าวแสดงสมบัติความเสถียรทางความร้อนที่ดีของฟิล์มบางเซอร์โคเนียมไนไตรด์ การเพิ่มขึ้นเซอร์โคเนียมระหว่างฟิล์มเซอร์โคเนียมไนไตรด์และวัสดุรองรับ ไม่ได้มีอิทธิพลต่อการเพิ่มขึ้นของความแข็ง ในทางตรงข้ามชั้นเซอร์โคเนียมสามารถช่วยในการยึดเกาะที่ดีขึ้นระหว่างเซอร์โคเนียมไนไตรด์และวัสดุรองรับ ชั้นเซอร์โคเนียมมีส่วนในการลดค่าความเค้นตกค้างและป้องกันฟิล์มลอกก่อน

จุฬาลงกรณ์มหาวิทยาลัย

ภาควิชา.....ฟิสิกส์.....  
 สาขาวิชา.....ฟิสิกส์.....  
 ปีการศึกษา.....2552.....

ลายมือชื่อนิสิต.....จิรวรรณ แสนทน.....  
 ลายมือชื่อ.ที่ปรึกษาวิทยานิพนธ์หลัก.....  
 ลายมือชื่อ.ที่ปรึกษาวิทยานิพนธ์ร่วม.....

## 4972250323: MAJOR PHYSICS

KEYWORDS: ZIRCONIUM NITRIDE / SPUTTERING / THIN FILM / ION-SURFACE INTERACTIONS

JIRAWAN SAENTON: GROWTH OF MULTIFUNCTIONAL ZIRCONIUM NITRIDE THIN FILMS BY REACTIVE DC MAGNETRON SPUTTERING. THESIS ADVISOR: ASST. PROF. SUKKANESTE TUNGASMITA, Ph.D., THESIS CO-ADVISOR: ASST. PROF. SAKUNTAM SANORPIM, Ph.D., 57 pp.

Zirconium nitride (ZrN) thin films have been deposited on silicon (100) substrates by reactive d.c. magnetron sputtering at various nitrogen partial pressures and different energies of ion bombardment during growth via substrate bias voltage. For optimized growth condition, the films grown with nitrogen partial pressure between 14-17% of total pressure, gave a stoichiometric composition ZrN material, which has a gold color. We found that the nitrogen partial pressure has major effects on the elemental composition of material, the deposition rate, crystal preferred orientation and color of the films. The energy of assisted-ions was varied between 8 to 108 eV. The energy of assisted-ions has slightly effects on stoichiometric composition but can help to increase the hardness and reduce the surface roughness. The ZrN (111) is a preferred orientation for all the growth conditions. The maximum hardness value of ZrN thin films is at 38.7 GPa, for the films that grown with using the energy of ions at 38 eV After annealing the films, the chemical composition of samples is just slightly changed but not the color of the films. This result indicates the good thermal stability of the ZrN thin films. The additional Zr interlayer between ZrN film and substrate does not influence to increase of the hardness. On the other hand, this layer can improve the adhesion between ZrN and substrate. This Zr interlayer may attribute to the decreasing of residual stress and prevent the film to peel off.

Department: .....Physics.....

Field of Study: ...Physics.....

Academic Year: ...2009.....

Student's Signature.....

Advisor's Signature.....

Co-Advisor's Signature.....

## Acknowledgements

I would like to express my gratitude to my advisor, Assistant Professor Dr. Sukkaneste Tungasmita and Assistant Professor Dr. Sakuntam Sanorpim for their valuable assistance, suggestion and encouragement throughout the course of this research.

I would like to thank Assistant Professor Dr. Kajornyod Yoodee and Dr. Burin Asavapibhop for serving as chairman and committee, respectively. Their comments on this thesis are also greatly appreciated. Special thank goes to Associate Professor Dr. Surasing Chaiyakun for help in the growth of films at Burapha University, valuable suggestions, teachings, and insights in sputtering processing.

I would like to thank Assistant Professor Dr. Patama Visuttipitukul for support in X-ray diffraction measurements. This work has been supported by The 90th Anniversary of Chulalongkorn University Fund (Ratchadaphiseksomphot Endowment Fund).

I would like to acknowledge Department of Physics, Faculty of Science, Chulalongkorn University for providing teaching assistantship. I would like to thank everyone in Advance Material Physics Research Group (AMPRG) for helping and friendship during this work. Especially, I want to thank Miss Pattira Homhoul for suggestion and help. Thank to all my friends at the Department of Physics for their fun and for a good relationship throughout my study.

Finally, I would like to express my deepest gratitude to my family; my father, my mother and my brother for their love, understanding, support and encouragement.

# Contents

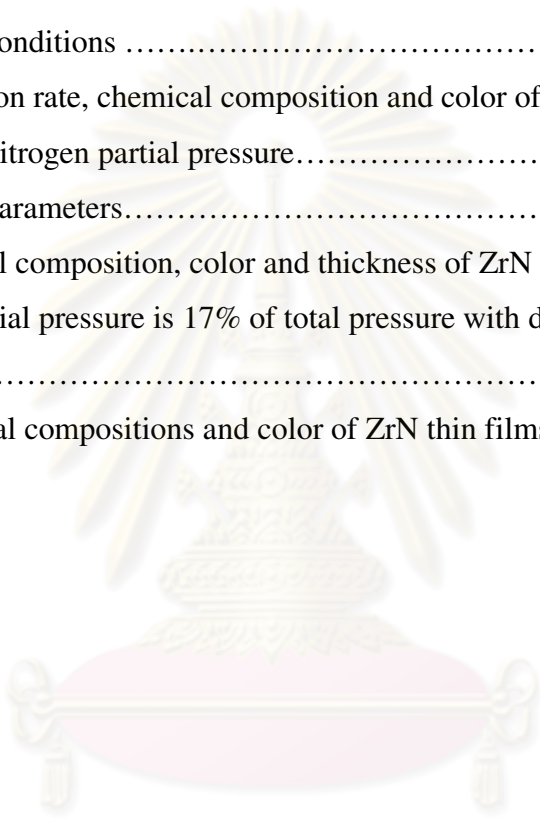
|   | Page       |
|---|------------|
| <b>Abstract (Thai)</b> .....  | <b>iv</b>  |
| <b>Abstract (English)</b> .....   | <b>v</b>   |
| <b>Acknowledgements</b> .....   | <b>vi</b>  |
| <b>Contents</b> .....   | <b>vii</b> |
| <b>List of Tables</b> .....   | <b>ix</b>  |
| <b>List of Figures</b> .....  | <b>xi</b>  |
| <br><b>Chapter</b>  |            |
| <b>I Introduction</b> .....   | <b>1</b>   |
| <b>II Theoretical Background</b> .....                                      | <b>3</b>   |
| 2.1 ZrN Thin Films.....   | 3          |
| 2.2 Concept of Sputtering.....  | 3          |
| 2.3 DC Glow Discharge.....  | 5          |
| 2.4 Ion - Surface Interactions at the Target.....                           | 6          |
| 2.5 Magnetron Sputtering Technique.....                                     | 7          |
| 2.6 Reactive Sputtering Process.....  | 9          |
| 2.7 Collision Processes of Two Particles.....                               | 11         |
| 2.8 Film Formation of Sputter Atomic Flux.....                              | 12         |
| 2.9 Ion - Surface Interactions on Surface Mobility.....                     | 15         |
| <b>III Characterizations of Thin Film</b> .....                             | <b>17</b>  |
| 3.1 X-Ray Diffraction.....  | 17         |
| 3.2 Scanning Electron Microscopy with Energy Dispersive X-ray Analysis..... | 18         |
| 3.3 Atomic Force Microscope.....  | 22         |
| 3.4 Nanoindentation.....  | 24         |

| <b>Chapter</b>  | <b>Page</b> |
|---|-------------|
| <b>IV Experiment, Results and Discussions.....</b>              | <b>29</b>   |
| 4.1 Substrate Preparation.....                                  | 29          |
| 4.2 ZrN Thin Films Synthesis.....                               | 29          |
| 4.3 Effects of the Nitrogen Partial Pressure.....               | 31          |
| 4.4 Effects of the Energetic Ions Assistance during Growth..... | 35          |
| 4.5 Effects of the Post- Annealing and Metallic Interlayer..... | 41          |
| <b>V Conclusions.....</b>                                       | <b>44</b>   |
| <b>References.....</b>  | <b>46</b>   |
| <b>Appendices.....</b>  | <b>51</b>   |
| <b>Appendix A Conference Presentations.....</b>                 | <b>52</b>   |
| <b>Appendix B Proceeding.....</b>                               | <b>53</b>   |
| <b>Vitae.....</b>   | <b>57</b>   |

ศูนย์วิทยทรัพยากร  
จุฬาลงกรณ์มหาวิทยาลัย

## List of Tables

| <b>Table</b>   | <b>Page</b> |
|--|-------------|
| 4.1 Deposition conditions .....  | 32          |
| 4.2 The deposition rate, chemical composition and color of the ZrN thin films as a function of nitrogen partial pressure.....  | 33          |
| 4.3 Deposition parameters.....   | 35          |
| 4.4 The chemical composition, color and thickness of ZrN thin films grown at the nitrogen partial pressure is 17% of total pressure with different the energy of ions..... | 36          |
| 4.5 The elemental compositions and color of ZrN thin films after annealing.....  | 41          |

  
 ศูนย์วิทยทรัพยากร  
 จุฬาลงกรณ์มหาวิทยาลัย

# List of Figures

| <b>Figure</b>  | <b>Page</b> |
|--|-------------|
| 2.1 Schematic of crystal structure for rocksalt ZrN.....   | 3           |
| 2.2 Schematic of a basic d.c. sputtering system.....   | 4           |
| 2.3 The relation between the current density and voltage in a d.c. glow discharge system.....  | 5           |
| 2.4 Momentum exchange processes at the target.....   | 6           |
| 2.5 Schematic of a magnetron sputtering source.....  | 8           |
| 2.6 Magnetic configurations in magnetron sputtering.....   | 8           |
| 2.7 Hysteresis curve during reactive sputtering.....   | 10          |
| 2.8 Schematic depiction of the binary collision.....   | 12          |
| 2.9 Formation of a thin film.....  | 13          |
| 2.10 Schematic representation of the influence of substrate temperature and argon working pressure on the structure of sputtered thin films..... | 14          |
| 2.11 Effect of bombarding ions on the surface atoms.....   | 15          |
| 3.1 Diffraction of X-ray from parallel planes in the crystal followed by Bragg's law.....  | 18          |
| 3.2 Types of interactions between an incident electron beam and the surface of sample.....   | 19          |
| 3.3 The electron interaction volume with in the sample.....  | 19          |
| 3.4 Schematic showing the production of characteristic X-rays.....   | 20          |
| 3.5 Schematic of atomic force microscope.....  | 23          |
| 3.6 Schematic diagram of nanoindentation.....  | 24          |
| 3.7 Schematic diagram of the typical load-displacement curve.....  | 25          |
| 3.8 Schematic representation of the indenter-sample contact.....   | 26          |
| 4.1 Schematic of ion-assisted reactive magnetron sputtering of zirconium nitride thin film.....  | 30          |
| 4.2 The colors of ZrN films deposited at difference nitrogen partial pressure.....   | 33          |

| <b>Figure</b>   | <b>Page</b> |
|---|-------------|
| 4.3 The X-ray diffraction patterns of the ZrN thin films with different stoichiometric.....   | 34          |
| 4.4 The X-ray diffraction patterns of the stoichiometric ZrN thin films grown with different the energy of assisted ions.....                         | 37          |
| 4.5 RMS surface roughness of the stoichiometric ZrN thin films grown with different the energy of assisted ions.....                                  | 38          |
| 4.6 The AFM images of ZrN films deposited with different assisted ions energy.....  | 39          |
| 4.7 The hardness of stoichiometric ZrN thin films grown with different the energy of assisted ions.....   | 40          |
| 4.8 The SEM images of ZrN and ZrN/Zr films after annealing at 350°C.....  | 42          |
| 4.9 XRD patterns of zirconium nitride thin films grown at different the energy of assisted ions, before and after annealing at 350°C for 60 min ..... | 42          |
| 4.10 The hardness of ZrN thin films grown at different the energy of assisted ions, before and after annealing at 350°C for 60 min .....              | 43          |

# CHAPTER I

## INTRODUCTION

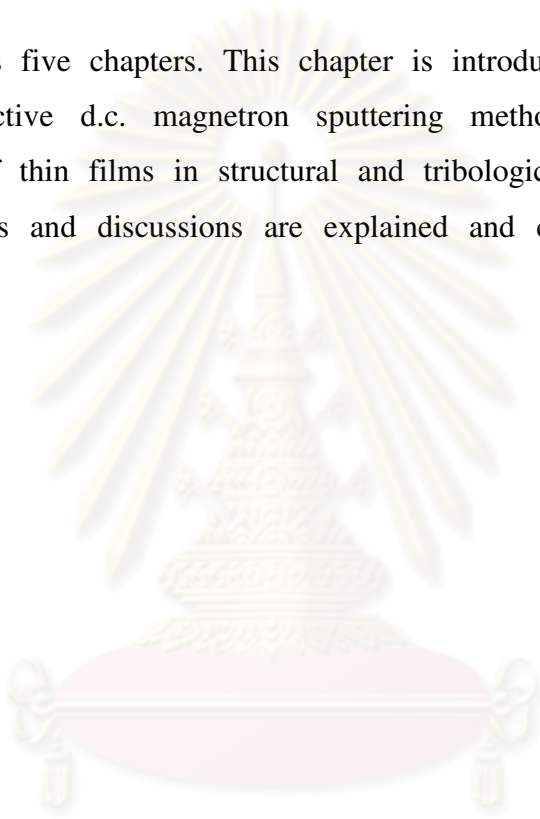
Transition metal nitrides films are widely used as diffusion barriers in microelectronics, hard coatings on cutting tools or as corrosion and abrasion resistant layers on optical and mechanical components. Among the different transition metal nitrides (TiN, CrN, HfN, TaN, etc.) zirconium nitride (ZrN) is another attractive material due to its good chemical and physical properties [1] such as high hardness (up to 40 GPa, approximately) [2], low electrical resistivity, high chemical and thermal stability [3], golden color, corrosion resistance [4], low friction coefficient, high melting point and biocompatibility [5]. The zirconium nitride films are used in many applications such as cutting tools for enhance the lifetime of the tools, medical tools, optical application for heat mirrors [6], diffusion barriers in semi-conductor technology, cryogenic thermometer [7] and decorative coating because of their high chemical stability and scratch resistance.

The zirconium nitride films can be prepared by several techniques such as arc evaporation, CVD, ion beam assisted deposition [8], chemical vapor deposition, reactive sputtering, pulsed laser deposition, plasma nitridation, vacuum arc deposition and ultra-high vacuum sputtering [9]. However, zirconium has a higher melting point, a lower vapor pressure and higher susceptibility of the contamination by oxygen and carbon. It is more difficult to deposit ZrN film than TiN or CrN films by evaporative physical vapor deposition (PVD) methods [10].

In this thesis work, the reactive d.c. magnetron sputtering is used for the deposition of zirconium nitride films. The nitrogen partial pressure and energy of bombarded ions on the surface of on-growing films by substrate bias voltage are growth parameters in our experiment. The nitrogen partial pressure has influence on different structures (ZrN, ZrN<sub>2</sub>, and Zr<sub>3</sub>N<sub>4</sub>) [11, 12], color and stoichiometric composition [13]. The energies of the ion bombardment on the surface of on-growing films have influence on crystal structure,

surface morphology, deposition rate and hardness [2, 14]. In addition, the ZrN thin films are annealed in Ar. The chemical composition, structure, surface morphology and mechanical properties are investigated. The aims of this thesis is to study the influence of growth parameter and find the optimize conditions for deposition of the zirconium nitride films.

The thesis has five chapters. This chapter is introduction, chapter 2 explains theoretical of reactive d.c. magnetron sputtering method. Chapter 3 describes characterizations of thin films in structural and tribological properties. Chapter 4, experimental results and discussions are explained and chapter 5 is conclusions, respectively.



ศูนย์วิจัยทรัพยากร  
จุฬาลงกรณ์มหาวิทยาลัย

# CHAPTER II

## THEORETICAL BACKGROUND

### 2.1 ZrN Thin Films

Zirconium nitride (ZrN) is a transition metal nitride in the family of other nitride thin films like TiN, HfN, CrN, TaN, etc. It has two phases: rocksalt structure, which is a stable phase (ZrN), as shown in figure 2.1 and orthorhombic structure, which is a metastable phase ( $\text{ZrN}_2$ ), ( $\text{Zr}_3\text{N}_4$ ) [11]. The lattice parameter is a 4.577 Å for rocksalt ZrN structure [15].

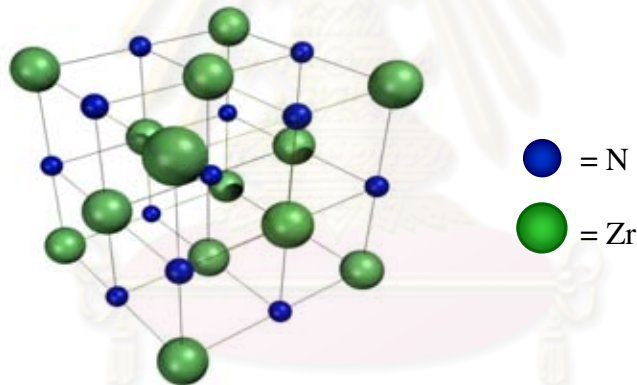


Figure 2.1: Schematic of crystal structure for rocksalt ZrN [16]

This material has many advantages for the modern industry. There are many research works that studied the structural and tribological properties of zirconium nitride thin films for a past few years [3, 6, 9, 11, 15, 17-21].

### 2.2 Concept of Sputtering

Sputtering is one of the most common methods for the deposition of thin films. The sputtering process is that the surfaces of the target are bombarded by energetic ions. The atom of target are eject from the surface due to collision of energetic ions. This

phenomenon is called “sputtering” which is applied for deposition of thin film. In process, there are energy and momentum transfer between ions and atoms of target. Figure 2.2 shows a schematic of a basic d.c. sputtering system. This system consists of chamber, d.c. power supply, vacuum system and gas feeding system. The target is connected to a d.c. power supply and opposite the substrate which can be grounded, floated, heated or biased. Prior to deposit, the system was pumped down to a base pressure then inert gas such as Ar for non-reactive sputtering is filled in the chamber. The high negative voltage is applied to the target and Ar gas is ionized ( $\text{Ar} \rightarrow \text{Ar}^+ + \text{e}^-$ ). The positive gas ions in plasma bombard the surface of the target then most neutral atoms of target eject from the target surface and kinetically move toward the substrate to form a film layer on the substrate

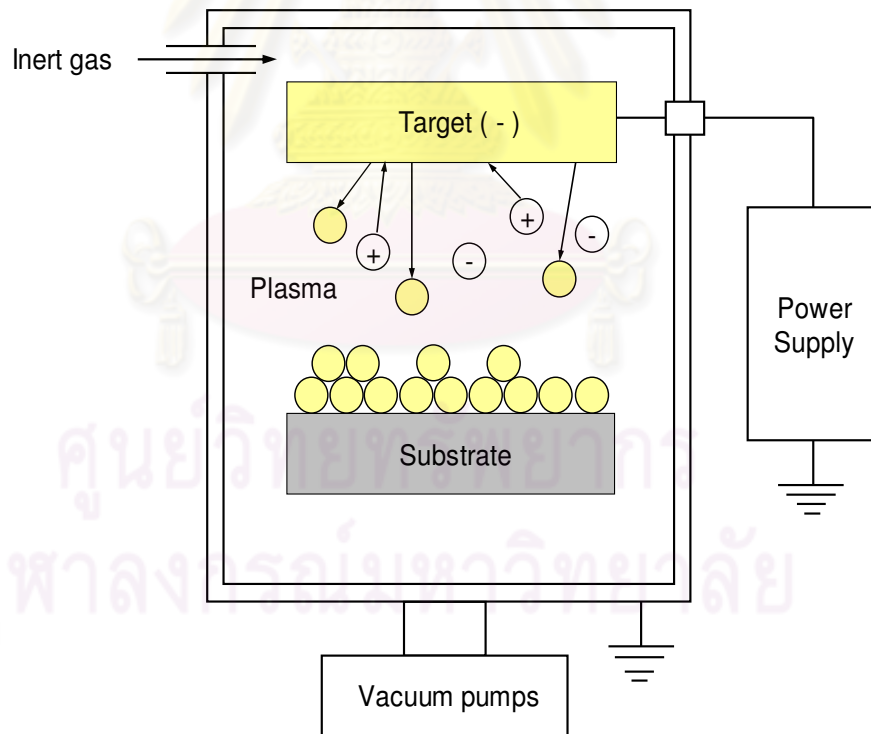


Figure 2.2: Schematic of a basic d.c. sputtering system

## 2.3 DC Glow Discharge

DC glow discharge sputtering is one of the simplest sputtering techniques. Figure 2.3 shows the relationship between current density and voltage in a d.c. glow discharge system.

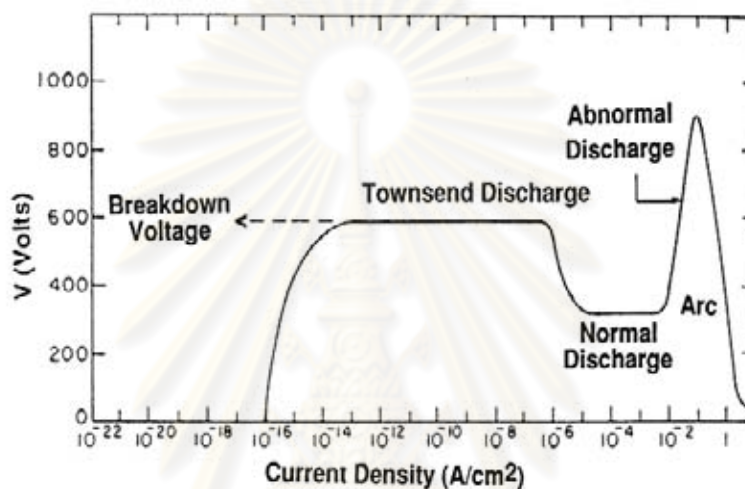


Figure 2.3: The relation between the current density and voltage in a d.c. glow discharge system [22]

At a dc power is applied to the target, initially a tiny current flows through the system due to a small number of charge carriers in the system. As the applied target voltage increases close to be break down voltage ( $V_B$ ), charge multiplication due to the neutral gas atoms are impacted by ions then gas particles ionize and the secondary electrons that are emitted from the target. The positive ions in the plasma are accelerated to the target (cathode) and the secondary electrons ions in the plasma are accelerated to the substrate (anode). As a result, the current rises and a *Townsend discharge* is created. This is the beginning of an avalanche which ions and electrons are increasable created. Then voltage rapidly increase leads to a steady state where the number of ions and electrons are produced becomes the same, the discharge becomes self-sustaining. Then, gas in system glow becomes to increase and accompany with the current sharp rise and

the voltage drop. This is the “normal glow” state. Initially, collision of ions on cathode is not uniform. As more power is applied, collision of ions covers over surface cathode until a nearly uniform current density is achieved. This is the “abnormal glow” state which is the operative domain for sputtering and other discharge process [22, 23].

## 2.4 Ion – Surface Interactions at the Target

When the target is bombarded by the ions, the following processes may occur:

- Ion or neutral atoms are reflected.
- Secondary electrons are emitted due to ion impact.
- Sputtered atoms are ejected from the target.
- The ions are buried in the target with/without the ejection of target atom.

Each interaction depends on the type of ions (mass, charge), the nature of surface atoms and ion energy. The interaction between the ion and the target atoms leads to the sputtering phenomena. The momentum of energetic particles is transferred to the target. The sputtered target atoms can be ejected when collisions occur at a certain number of times. These collisions change the direction of momentum transfer towards the target surface.

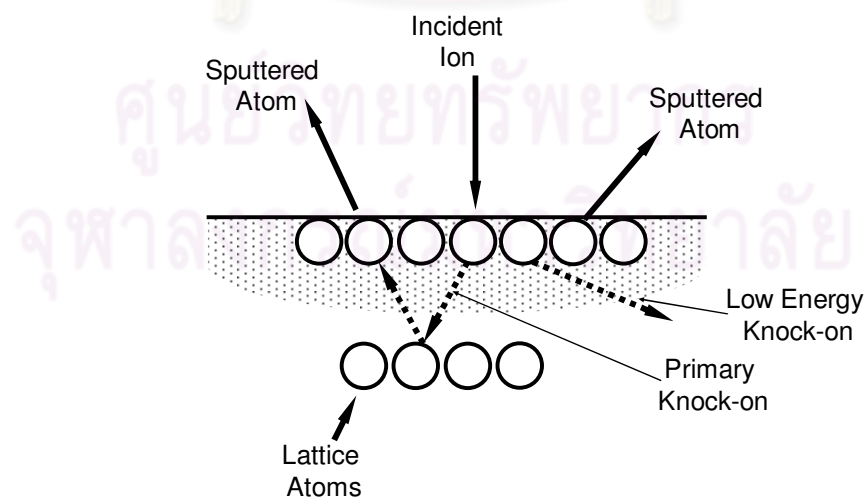


Figure 2.4: Momentum exchange processes at the target [22]

The momentum exchange processes are shown in figure 2.4 and could include a low energy knock-on process which the target surface atom receives only a glancing blow and transfers its energy to the neighboring surface atoms. Then, sputtered atoms are ejected from the target. On the other hand, a primary knock-on atom can undergo several collisions inside the target before transferring the momentum that cause the sputtering; or the primary knock-on can itself be reflected back and hit the surface atoms [22].

## 2.5 Magnetron Sputtering Technique

The limitation of the basic diode sputtering is low ionization efficiencies in the plasma and high heating effect of substrate. Therefore the magnets are use in the sputtering process to increase the ionization by the magnetic field that trapped electrons near the target surface. This technique is called “Magnetron Sputtering”. The magnetron sputtering system is illustrated in figure 2.5. The magnets are place behind the target. There are two poles of magnet are use for configurations in magnetrons. One pole is at the center of the target and the second pole is at around the outer edge of the target. Magnetic fields are mainly parallel to the target surface. Thus, the secondary electrons which are emitted from the target are trapped near the target surface. This cause results in a large increase of ionization above the target surface. The motion of the secondary electrons following by the Lorentz forces.

The electron is travelling at an angle  $\theta$  to magnetic field ( $\mathbf{B}$ ) with the velocity ( $v$ ). Then it will be controlled by a magnitude of  $\sin \mathbf{B}ev\sin \theta$  perpendicular to the field. If there is no collision, the electron will move with circular motion around  $\mathbf{B}$  at the radius given by

$$\frac{m_e v (\sin \theta)^2}{r} = \mathbf{B}ev\sin \theta, \quad (2.1)$$

$$\text{or} \quad \frac{m_e v \sin \theta}{\mathbf{B}e} = r, \quad (2.2)$$

coupled with the velocity  $v \cos \theta$  parallel to  $\mathbf{B}$ , the motion will be a helix.

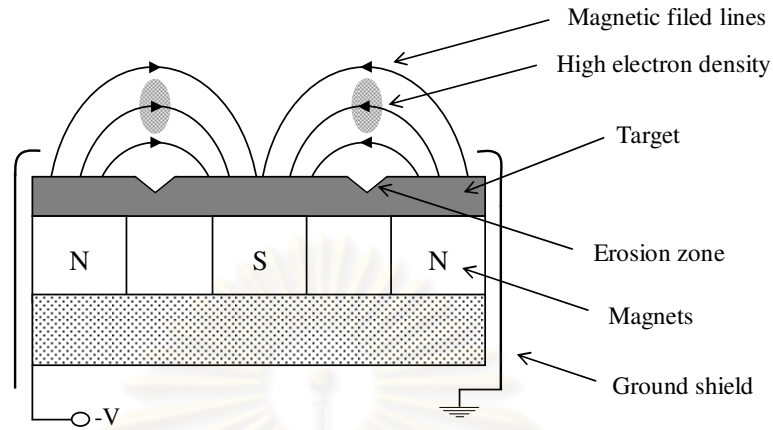


Figure 2.5: Schematic of a magnetron sputtering source [24]

The magnetrons can be classified into 3 types according to their magnetic configurations, as shown in figure 2.6: balanced magnetron, unbalanced magnetron type I, and unbalanced magnetron type II [24].

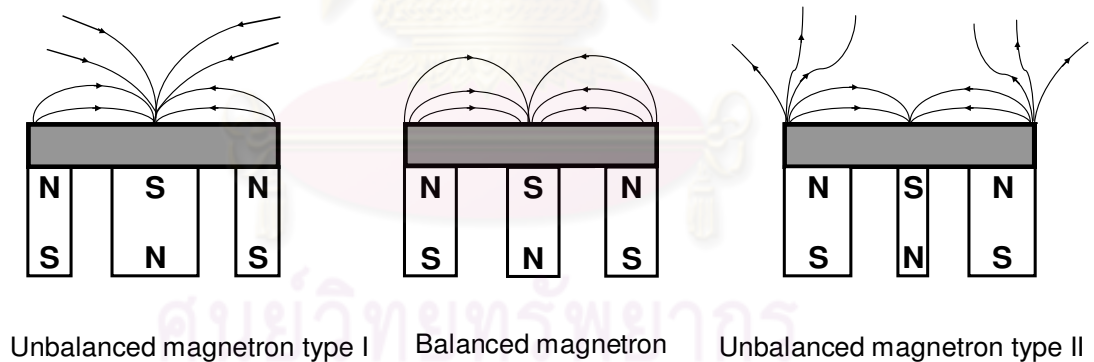


Figure 2.6: Magnetic configurations in magnetron sputtering [24]

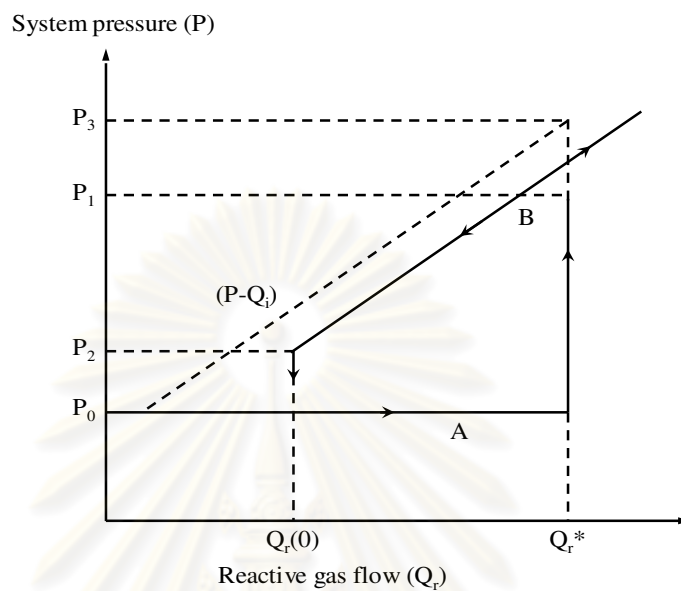
In the case of a balanced magnetron, the centre and outer poles are equally strong. The magnetic field lines are controlled close to the target surface. The plasma density is limited in regions near the target. In the case of an unbalanced magnetron type I, the centre pole is stronger than the outer poles. The magnetic field lines are directed towards chamber walls and the plasma density in the substrate region is low. This design is not

commonly used because the lower ion current at the substrate. The plasma density is low in regions of the substrate. For an unbalanced magnetron type II, the outer pole is stronger than the centre pole. The magnetic fields are closed between the centre and outer pole and some magnetic fields direct toward the substrate. Some secondary electrons travel to the substrate by the magnetic field lines. This case is advantageous for increasing ion current at the substrate, which increases ion bombardment of the substrate will affect the properties and structure of the film. The unbalanced magnetron type II has been used in the growth of ZrN thin films this work.

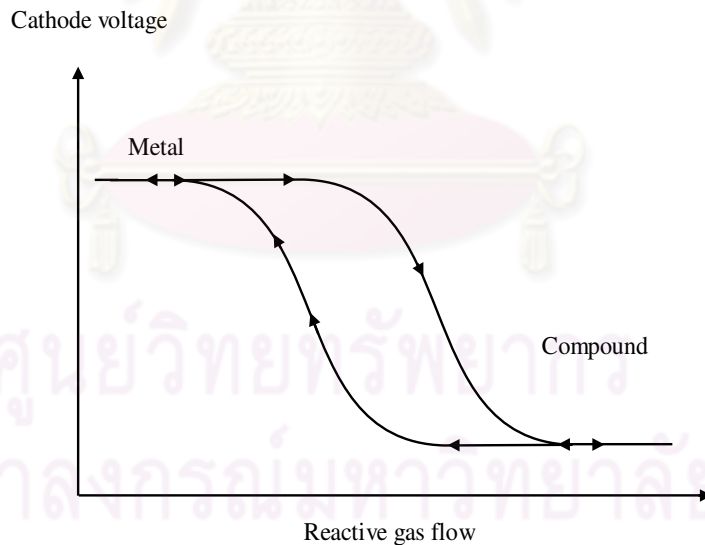
During the sputter process a magnetic field can be used to trap secondary electrons close to the target. The electrons follow helical paths around the magnetic field lines and impact with neutral gaseous near the target. This enhances the ionization of the plasma near the target leading to a higher sputter rate.

## 2.6 Reactive Sputtering Process

In sputtering deposition in an inert gas (usually argon) with metal target, the metal thin films can be formed. For reactive sputtering, non-inert gas such as  $O_2$ ,  $N_2$  and  $CH_4$  as reactive gas which is added to the plasma. This process is called “reactive sputtering” which is a method for formation of compound thin film from the chemical reaction between the metal targets and reactive gases. The metal target can be sputtered in reactive gases to form a compound thin film. Reactive sputtering also includes sputtering from a compound target. The chemical reaction generally occurs at the surface. This could be on the target surface or the substrate. As the partial pressure of reactive gas increases, the chemical reaction will occur at the surface of the target, resulting in compound formation on the surface of the target and the sputtering rate decrease. This is referred to as the non-metallic or poisoned mode of sputtering as the target is in “poisoned” state [22]. The effect is generally described in terms of a hysteresis. Figure 2.7 (a) shows hysteresis curve for the total system pressure ( $P$ ) and the flow rate of reactive gas ( $Q_r$ ) in the system [23].



(a)



(b)

Figure 2.7: Hysteresis curve during reactive sputtering (a) Hysteresis curve for system pressure vs. reactive gas flow rate during reactive sputtering (b) Hysteresis curve of cathode voltage vs. reactive gas flow rate at constant discharge current [23]

The system use only inert gas ( $Q_i$ ) such as Ar. The dotted line represents the variation of P and flow rate of inert gas ( $Q_i$ ). As  $Q_i$  increase, P increases because the constant pumping speeds. When the reactive gas ( $Q_r$ ) such as  $N_2$  is filled in the system. As the flow rate increase from  $Q_r(0)$ . The total pressure is remain constant at initial value  $P_0$  due to the reactive gas ( $N_2$ ) react with the target surface and remove from the gas state. Then the flow rate increase to the critical flow rate ( $Q_r^*$ ) the system pressure jumps to the new pressure ( $P_i$ ). If the compound on the surface target is not sputtered, the system pressure would be higher such as  $P_3$ . The equilibrium value of P is started. The change in  $Q_r$  effect to P such as it can be increase or decrease linearly as show. As  $Q_r$  decrease sufficiently, P reaches the initial pressure again.

## 2.7 Collision Processes of Two Particles

In plasma reactions, collision between electron and species (charge and neutral) are required. Elastic or inelastic collision depends on the internal energy of the collision species, which is conserve or not. In the elastic collision, momentum and kinetic energy are conserved. Only kinetic energy is exchange. In this case, all atoms are not excitation and potential energy conserved. The result for elastic binary collision is [23, 25]

$$\frac{E_2}{E_1} = \frac{4M_1M_2}{(M_1+M_2)^2} \cos^2\theta , \quad (2.3)$$

where  $M_1$ ,  $M_2$  are mass and  $E_1$ ,  $E_2$  are energy of the particles. Figure 2.8 shows a schematic depiction of the binary collision.

Let mass  $M_1$  is move particle with  $v_1$  and mass  $M_2$  is stationary particle. The collision occurs at an angle theta to the line joining the centers of mass at contact. The quantity  $\frac{4M_1M_2}{(M_1+M_2)^2}$  is known as the energy transfer function. In this case, an electron colliding a stationary nitrogen molecule,  $M_1$  (electron mass) is less than  $M_2$  (gas molecule). Thus the energy transfer function is about  $4M_1/M_2$  and has a value about  $10^{-4}$  so a little kinetic energy is transferred in the collision.

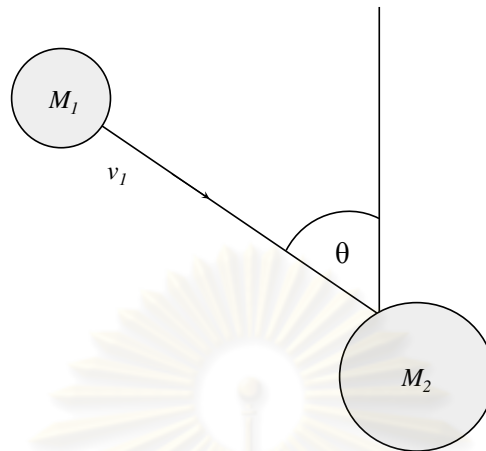


Figure 2.8: Schematic depiction of the binary collision

In the inelastic collision, the kinetic energy of electron can be transferred to heavier specie

$$\frac{\Delta U}{\frac{1}{2} M_1 v_1^2} = \frac{M_2}{(M_1 + M_2)^2} \cos^2 \theta, \quad (2.4)$$

where  $\Delta U$  is the change in internal energy,

$v_1$  is the initial velocity of particle 1.

## 2.8 Film Formation of Sputter Atomic Flux

Thin films form through a nucleation and growth process, as shown in figure 2.9. The process begins as sputtered atomic flux arrives at the substrate, as in process A. These adatoms diffuse on the substrate or re-evaporate, as in process B. In process C the adatom interacts with another adatom, they are called cluster which has lower diffusion and more stable than single atom. The mobility of sputtered atom at the substrate depends on binding energy between atom with the substrate and substrate temperature. At higher substrate temperatures, the mobility of the adatom increase. Then more sputtered atoms arrive at the surface, the adatoms form triplets, quadruplets and so on. This is the nucleation stage of thin film growth and will begin to grow, as in process D, E and F respectively. Next, the certain size of clusters, which is called “Island”, is formed. These island grow large enough until they touch, this process is call the called “Coalescence”,

as in process G. The coalescence proceeds until the film reaches continuity, as in process H.

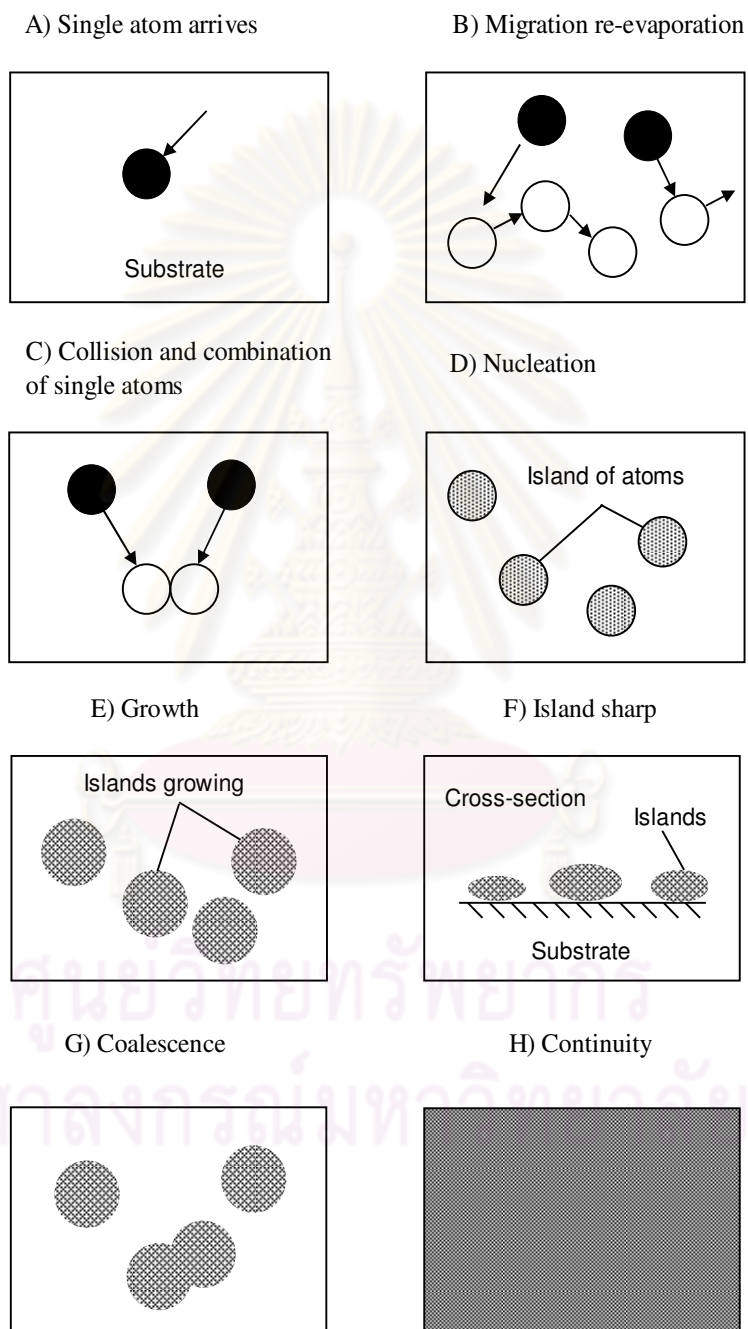


Figure 2.9: Formation of a thin film [25]

From observation in transmission electron microscopy (TEM), it appears that the island often displays liquid like behavior during coalescence. There are often crystallographic orientations as a result of competition between the structures of the coalescing island. During the island stage, each island is a single crystal when the substrate is single crystal such as Si. Otherwise, on polycrystalline substrate, the orientation of each island will be random. Therefore, the film is polycrystalline [25].

In most cases, thin films are formed by the coalescence of islands. When these islands grow together, various defects and grain boundaries are formed. Grains that coalesce with randomly oriented directions will produce a polycrystalline film. The figure 2.10 shows the structure zone model of Thornton, investigated the structures of thick films and determined that film structure could be expressed as a function of deposition temperature, melting temperature ( $T/T_m$ ) and deposition pressure.

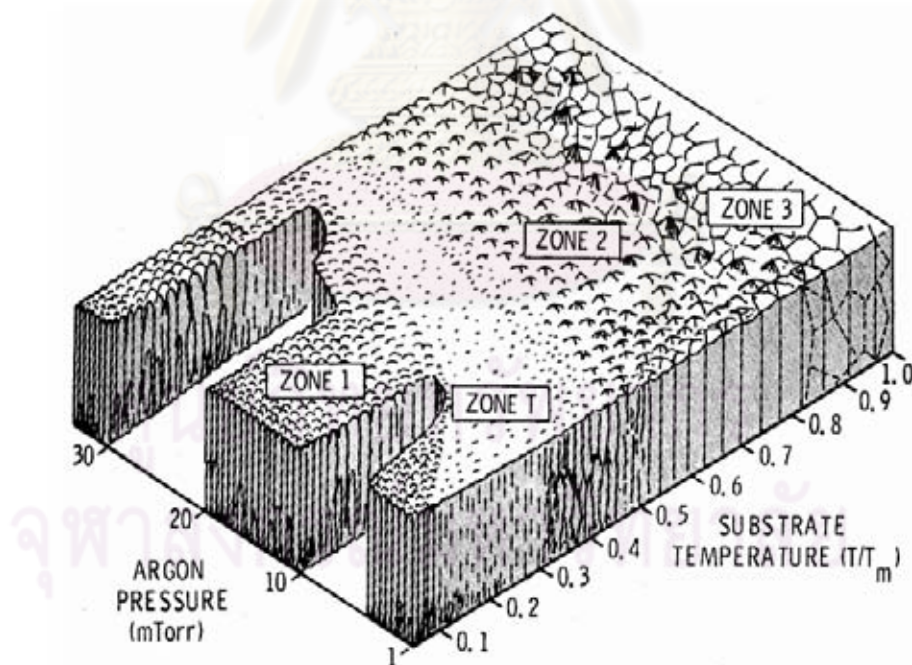


Figure 2.10. Schematic representation of the influence of substrate temperature and argon working pressure on the structure of sputtered thin films [26]

The diagram consists of four zones as seen in figure. Zone 1 films occur when adatom mobility is not enough to overcome the effects of shadowing and results in a fibrous film separated by voids. As  $T/T_m$  increases, therefore too does the crystallite size. Zone T is known as the transition region where the adatom mobility is sufficient to overcome the shadowing effects and results in a smoother surface than in Zone 1 films. Zone 2 is a region dominated by surface diffusion growth with increasing grain size separated by intercrystalline boundaries. Zone 3 is a region characterized by elevated growth temperatures. At these temperatures adatom mobility results in bulk diffusion. At sufficiently high substrate temperatures and sufficiently lattice matched substrates, epitaxial growth can be achieved [26].

## 2.9 Ion - Surface Interactions on Surface Mobility

The quality of the film can be improved by ion in the plasma which can be control by applying a bias on the substrate. This process is called “bias sputtering”. In general, a negative voltage is applied to the substrate. Therefore positive gas ions, which are near the substrate surface, are accelerated toward the substrate. The energy of the ions bombarding the substrate can be control by varying the bias voltage. With increasing substrate bias, there by surface mobility of adatom can be increased with out increasing of the deposition temperature.

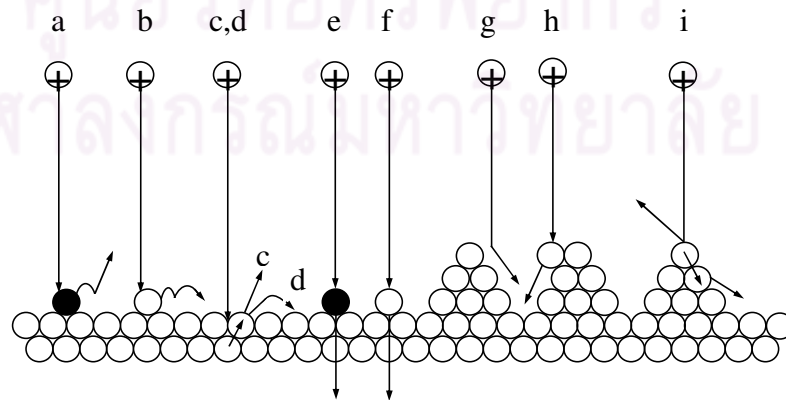
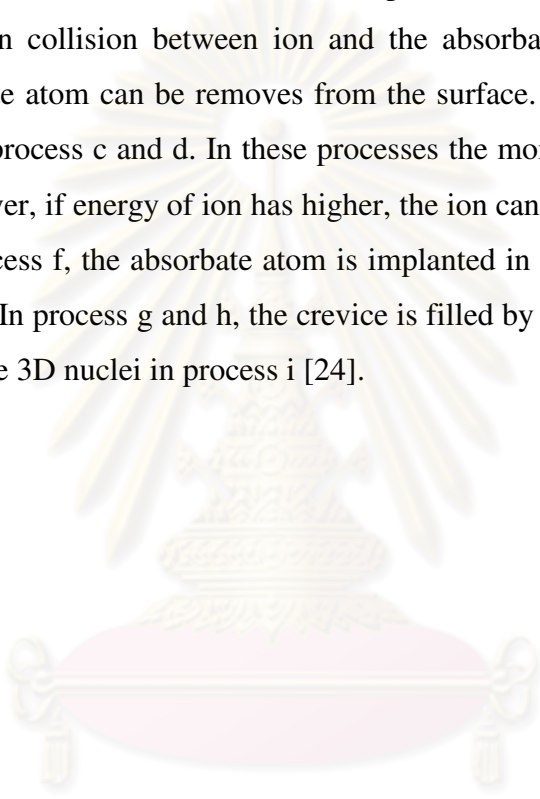


Figure 2.11: Effect of bombarding ions on the surface atoms [24]

There are many interactions on the surface from ion bombardment in low energy. The most important interactions between the ions and the surface atoms are atomic displacement, which is shown in figure 2.11. In process a, the absorbate atom is reflected due to collision of ion bombarding. It has received enough energy from an ion impact to break atomic bond of the surface and desorbs. In process b, the absorbate atom removes on the surface when collision between ion and the absorbate atom occurs. At higher energy, the absorbate atom can be removes from the surface. This case effect to surface vacancy created in process c and d. In these processes the momentum is transfer through the collision. However, if energy of ion has higher, the ion can be implanted in the film as in process e. In process f, the absorbate atom is implanted in the film due to it is collide by ion bombarding. In process g and h, the crevice is filled by the ion and sputtered atom. The ion disperses the 3D nuclei in process i [24].



ศูนย์วิทยทรัพยากร  
จุฬาลงกรณ์มหาวิทยาลัย

# CHAPTER III

## CHARACTERIZATIONS OF THIN FILM

In this work, ZrN thin films were characterized by many characterization techniques. Rigaku SA-HFM3 X-ray diffraction (XRD) is employed to determine the structure, phases and textures of the films. The chemical composition of the films is characterized by Oxford's INCA energy dispersive spectroscopy (EDS). The surface morphology and roughness of the films are determined by the JEOL JSM-6480LV scanning electron microscope (SEM) and Veeco Nanoscope - IV atomic force microscopy (AFM). CSM™ Berkovich diamond tip nanoindenter is used to measure the hardness of the films. A brief information on those techniques will be described in this chapter.

### 3.1 X-Ray Diffraction

X-ray diffraction (XRD) is a non-destructive technique that reveals detailed information about the crystal structure, chemical composition, and the structural properties such as preferred orientation and defect structure of materials and thin films. As the crystal lattice is a regular three-dimensional distribution (cubic, rhombic, etc.) of atoms in space. These are arranged so that they form a series of parallel planes separated from one another by a distance  $d$ , which varies according to the nature of the material. For any crystal, planes exist in a number of different orientations - each with its own specific  $d$ -spacing.

When a monochromatic X-ray beam with wavelength  $\lambda$  is projected onto a crystalline material at an angle  $\theta$ , diffraction occurs only when the distance traveled by the rays reflected from successive planes differs by a complete number ( $n$ ) of wavelengths, as shown in figure 3.1. By varying the angle  $\theta$ , the Bragg's Law conditions, are satisfied by different  $d$ -spacing in crystalline material.

$$2d \sin \theta = n \lambda, \quad (3.1)$$

where  $d$  is a spacing between atomic planes in the crystal,

$\lambda$  is wavelength of X- ray beam,

$\theta$  is the angle between the incident beam and the scattering planes,

$n$  is an integer.

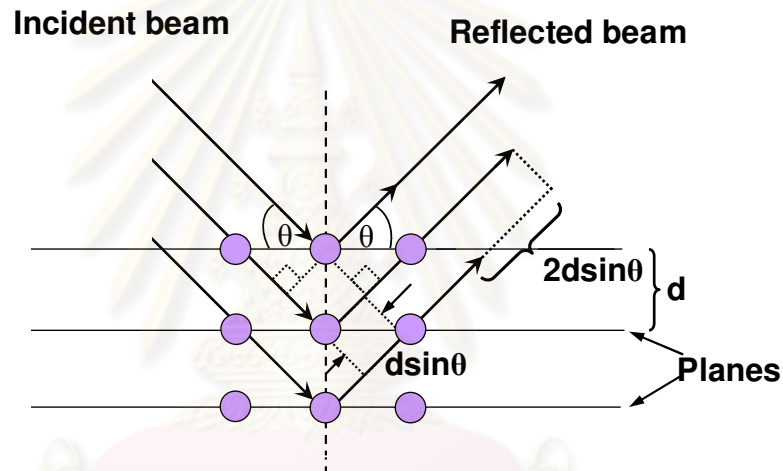


Figure 3.1: Diffraction of X-ray from parallel planes in the crystal followed by Bragg's law.

## 3.2 Scanning Electron Microscopy with Energy Dispersive

### X-ray Analysis

The scanning electron microscope (SEM) is a type of electron microscope that uses electrons instead of light to form an image. As an incident electron beam strikes the surface of sample, these interactions generate a variety of signals at the surface and sub-surface layers of sample; for example, secondary electrons, backscattered electrons, transmitted electrons, X- ray, light (cathodluminescence) and auger electrons [27], as shown in figure 3.2.

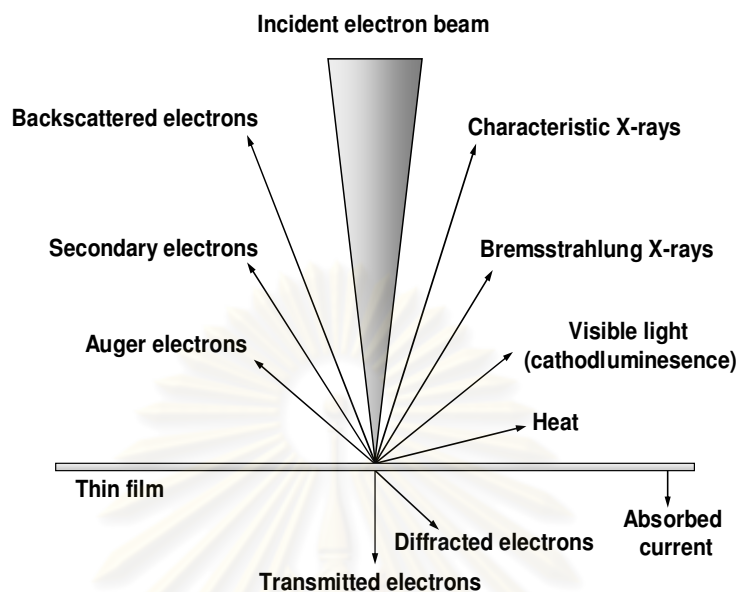


Figure 3.2: Types of interactions between an incident electron beam and the surface of sample [28]

During interactions, the volume that contains interactions which occurred due to the electrons penetration into the sample is called the interaction volume or excitation volume. The interaction volume varies with accelerating voltage and average atomic number of sample, as shown in figure 3.3.

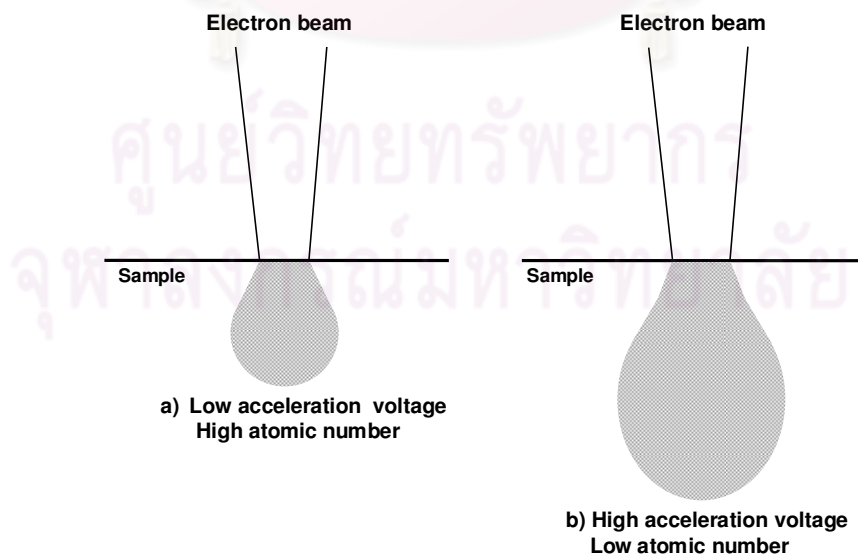


Figure 3.3: The electron interaction volume with in the sample [29]

These parameters affect to the shape and depth of the interaction volume inside the sample. At higher voltage, the interaction volume is larger and deeper. At higher atomic number materials absorb or stop more electrons and the interaction volume have a smaller. Within this volume, free electrons and the electromagnetic radiation are produced.

The secondary electrons are ejected from the valence band of the atoms by inelastic scattering interactions with incident electron beam. The secondary electrons are produced near the surface sample, with in 10 nm. The average energy of secondary electrons is about 3-5 eV. These secondary electrons emitted from the surface of sample to vacuum and then they are detected to create a surface picture by a detector. The secondary electrons are most valuable for showing morphology and topography of the samples [29].

The chemical composition of the samples can be determined by measuring energy of the characteristic X-ray produce, which this technique is called Energy Dispersive X-ray Spectroscopy, EDS or EDX. Interactions of an electron beam with the sample produces a variety of emissions, including characteristic X-rays. The characteristic X-rays occur from the inelastic collision between the primary electron and an electron in the inner-shell such as K shell, as shown in figure 3.4.

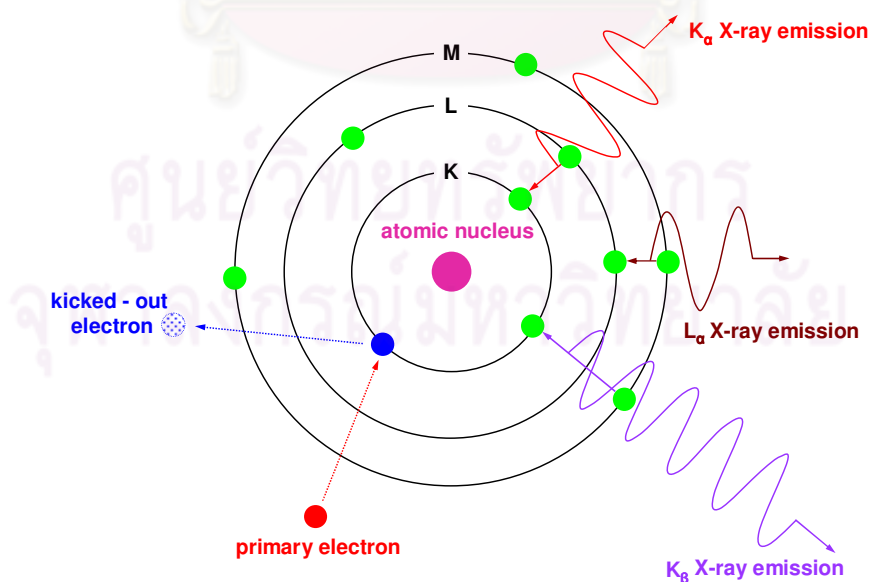


Figure 3.4: Schematic showing the production of characteristic X-rays [30]

When the sample is bombarded by the primary electron, there is energy transfer to an electron. An electron has higher energy than binding energy of electron in K shell, so it is knocked out of this shell. A vacancy in the K shell is filled by an electron from a higher energy level such as L, M shell. During the transition, the characteristic X-ray is emitted. The energy of X-ray corresponds to the difference in energy between the K shell that is vacant and the higher energy level that an electron falls. Each X-ray is called by follow the name of the shell (K, L, M) which creates the vacancy and a subscript is called by follow the number of shell jump by electron that filled the vacancy. Hence, a one shell jump is denoted by  $\alpha$ , a two shell jump is denoted by  $\beta$  and a three shell jump is denoted by  $\gamma$ . Example, a vacancy in K shell filled by an electron from the L shell would create a  $K_{\alpha}$  X-ray [29].

The weight or atomic percent of the samples can be calculated from the area under the peaks. At first, the background noise in the EDS spectrum is subtracted. Then, the count rate is compared to the count rate of the reference sample

$$k_l = \frac{I_l}{I_{ref}}, \quad (3.2)$$

where  $k_l$  is the fraction of the count rate,

$I_l$  is the count rate of sample with unknown composition,

$I_{ref}$  is the count rate of sample with known composition,

index  $l$  is the element and transition concerned.

However, there are many dependent factors which involve in the calculation of composition in the sample, the correction factors, so called “ZAF correction”, and are applied in the calculation.

The Z factor refers to the atomic number correction. This effect consists of two components: backscattering and stopping power. When the primary electron strikes the sample, some of the electrons will interact with the nucleus of the sample atoms. Then the backscattered electrons are reflected or back-scattered out of the sample surface by elastic scattering interactions with sample atoms. Since heavy elements (high atomic

number) backscatter electrons more strongly than light elements (low atomic number). Stopping power is the ability of a material to reduce the energy of an incident electron by inelastic scattering. The stopping-power is not constant but drops with increasing of the atomic number. This factor depends on the composition in the excitation volume.

The A factor refers to the absorption correction. Due to X-ray radiation from different elements will be generated in different depth in the sample. This factor is dependent on the excitation volume size and shape (geometry).

The F factor refers to fluorescence correction. The X-ray is produced within the sample by the bombarding primary electrons and has the ability for producing a second generation of X-rays. This is secondary fluorescence, generally shortened to fluorescence. This occurs when the X-ray has an energy greater than the critical excitation energy of another element present in the specimen. This factor depends on the composition in the excitation volume.

So, the real concentration is

$$C_I = k_I ZAF \quad (3.3)$$

### 3.3 Atomic Force Microscope

The atomic force microscope (AFM) is one type of scanning probe microscopy (SPM) which is used to scan the surface. The resolution of AFM is in rang 0.1 nm or less. In this work, AFM is use to obtain the image and surface information. AFM operate by measuring attractive or repulsive force between the tip and the sample. The tip of AFM is mounted at the end of cantilever and is used to scan the sample surface. A laser beam is directed toward the cantilever. The reflected beam of the laser from cantilever is detected by photodetector, as shown in figure 3.5. Interaction force between the tip and the surface make a deflection of the cantilever according to Hooke's law as show in equation 3.4. The photodetector measures the cantilever deflection in vertical. Then, the signal is transformed to create an image of surface [29].

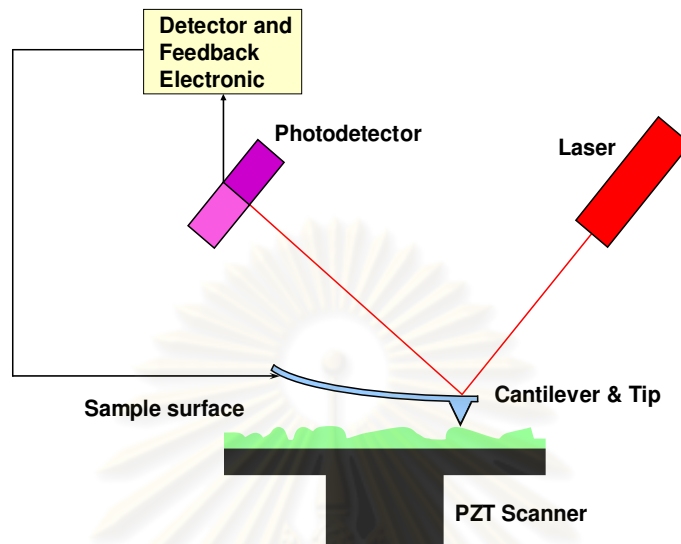


Figure3.5: Schematic of atomic force microscope [31]

$$F = - kz , \quad (3.4)$$

where  $F$  is the force,

$k$  is the spring constant of the cantilever

$z$  is the displacement of the cantilever.

In this work, “*Tapping mode*<sup>TM</sup>” AFM is used. During tapping mode operation, the cantilever oscillation amplitude is constant. When the tip passes over a bump or a cavity in the surface, the force acting on the cantilever will change the spring constant of cantilever, causing a change in the oscillation amplitude. The oscillation amplitude of the tip is measured by the detector and input to the controller electronics. Tapping Mode prevents the tip from sticking to the surface and causing damage during scanning. The surface information such as root mean square (RMS) surface roughness can be calculated from AFM analysis. RMS roughness is a standard deviation of the surface height within a given area define as [32]

$$RMS = \sqrt{\frac{\sum_{i=1}^N (Z_i - Z_{ave})^2}{N}}, \quad (3.5)$$

where  $Z_{ave}$  is the average surface height within the given area,

$Z_i$  is the current surface height,

$N$  is the number of point within a given area.

### 3.4 Nanoindentation

In this work, the CSM™ nanoindenter tester is used to determine the hardness and elastic modulus of the ZrN films. Nanoindentation is mainly consisted of a magnetic loading actuator, a capacitive displacement sensor, a probe, and a sample stage, as shown in figure 3.6.

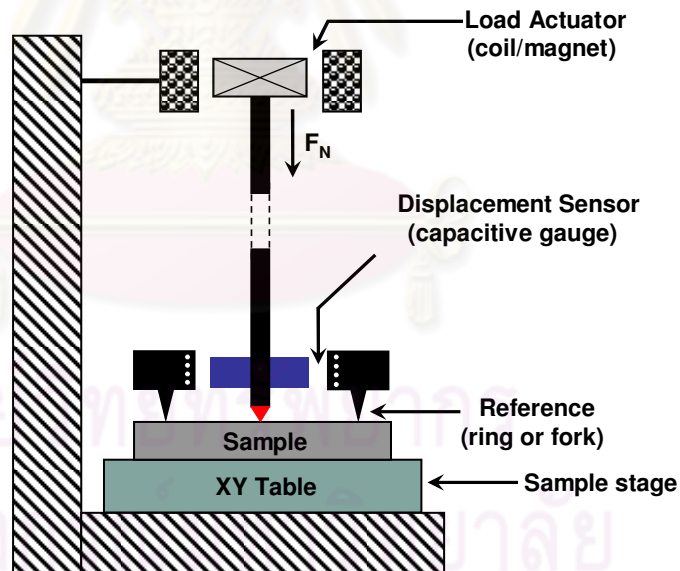


Figure 3.6: Schematic diagram of nanoindentation

When the indenter is driven into the material, the permanent indent could be happen on the material follow in the geometry indenter tip. The permanent indent is measured for calculate the contact area at maximum load. Thus, the hardness and elastic modulus are

obtained by dividing the maximum applied load by the contact area. In the nanoindentation technique, hardness and elastic modulus can be determined by the Oliver and Pharr method, where hardness ( $H$ ) can be defined as [33]

$$H = \frac{P_{max}}{A}, \quad (3.6)$$

where  $P_{max}$  is the maximum applied load,

$A$  is the contact area at maximum applied load.

The typical load-displacement curve, showing the values used in the Oliver and Pharr method [33], as show in figure 3.7.

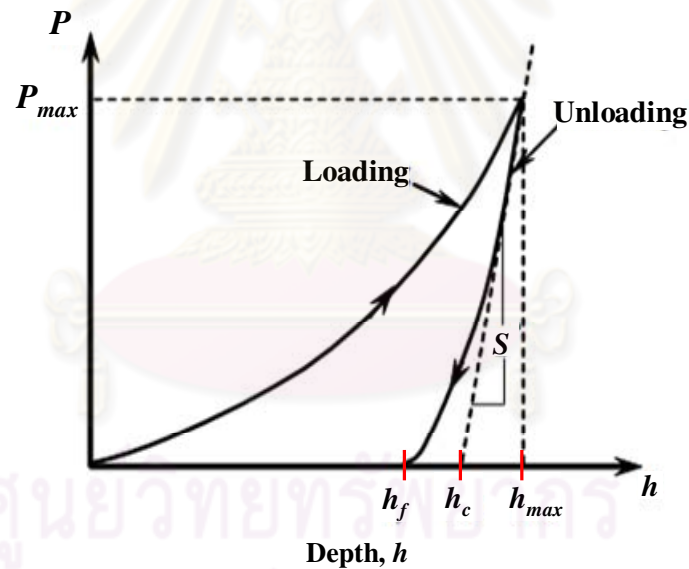


Figure 3.7: Schematic diagram of the typical load-displacement curve [34]

where  $h_f$  is the final unloading depth,

$h_{max}$  is the maximum indentation depth at maximum applied load,

$P_{max}$  is the maximum applied load,

$h_c$  is the contact depth.

$S$  is the slope of the tangent line to the unloading curve at the maximum applied load point ( $h_{max}$ ,  $P_{max}$ ) and is the contact stiffness.

The contact stiffness ( $S$ ), as defined is [33]

$$S = \left( \frac{dP}{dh} \right)_{(h_{max}, P_{max})}, \quad (3.7)$$

As the indenter is driven into the material, both elastic and plastic deformation caused the formation of an impression conforming to the shape of the indenter tip to some the contact depth,  $h_c$ . As the indent is withdrawn, only the elastic portion of the displacement is recovered. According to the recovery of the material, the elastic modulus is determined [35]. Figure 3.8 shows the schematic representation of the indenter-sample contact.

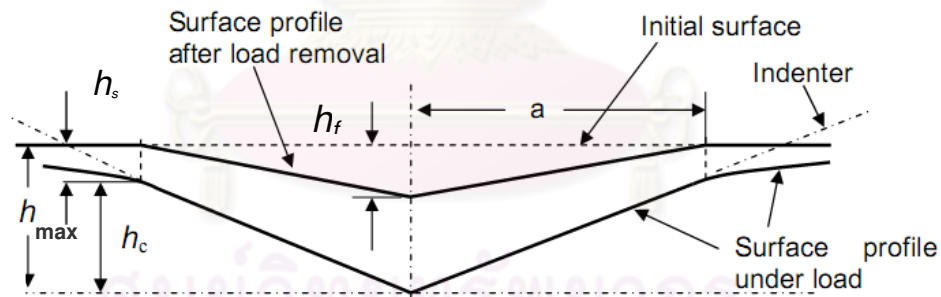


Figure 3.8: Schematic representation of the indenter-sample contact [36]

The reduced modulus ( $E_r$ ), accounting for the deformation of both indenter tip and material, can be calculated by

$$E_r = \frac{\sqrt{\pi} S}{\sqrt{A} 2}, \quad (3.8)$$

where  $S$  is the contact stiffness at the maximum applied load,  
 $A$  is the contact area at maximum applied load.

In addition, the elastic modulus of the material ( $E$ ) is expressed as

$$\frac{1}{E_r} = \frac{(1-\nu^2)}{E} + \frac{(1-\nu_i^2)}{E_i}, \quad (3.9)$$

where  $E$  is the elastic modulus of material,  
 $\nu$  is the Poisson's ratio of material,  
 $E_i$  is the elastic modulus of the indenter tip,  
 $\nu_i$  is the Poisson's ratio of the indenter tip.

In this work, Berkovich indenter is use in the indentation tester. For a perfect Berkovich indenter, the contact area at maximum applied load ( $A$ ) from Eq. (3.6) can be obtained by

$$A = 3\sqrt{3} \tan^2\theta h_c^2, \quad (3.10)$$

where  $\theta$  is face angle (Berkovich indenter  $\theta = 65.27^\circ$ ), evaluates to:

$$A \approx 24.5 h_c^2, \quad (3.11)$$

The contact depth  $h_c$  is given by

$$h_c = h_{max} - \frac{\varepsilon P_{max}}{S}, \quad (3.12)$$

where  $\varepsilon$  is associated with the specific tip geometry (Berkovich indenter  $\varepsilon = 0.75$ ) [33].

When the load-penetration depth data are obtained, the elastic modulus ( $E$ ) and hardness ( $H$ ) can then be calculated from Eq. (3.6)-(3.12). Firstly, the stiffness ( $S$ ) can be

calculate from the slope of the tangent line to the unloading curve at the maximum applied load point ( $h_{max}, P_{max}$ ) and the stiffness ( $S$ ) is used to calculate the contact depth ( $h_c$ ) (see Eq. (3.7)). Then the contact depth ( $h_c$ ) is used to calculate the contact area ( $A$ ) from the shape area function of the tip (see Eq. (3.12)). Finally, the stiffness ( $S$ ) and contact area ( $A$ ) are used to calculate the reduced modulus ( $E_r$ ), elastic modulus ( $E$ ) and hardness ( $H$ ) by using Eq. (3.8), (3.9) and (3.6), respectively.



# CHAPTER IV

## EXPERIMENT, RESULTS AND DISCUSSIONS

### 4.1 Substrate Preparation

In this thesis, zirconium nitride thin films (ZrN) were deposited on silicon (100) substrates by ion-assisted reactive d.c. magnetron sputtering. Prior to the deposition process, the substrates were chemically cleaned in trichloroethylene, acetone and isopropanol, respectively. Then, the substrates were blown to dry with nitrogen before introducing into vacuum chamber. After that, the system was pumped down to high vacuum stage at about  $5 \times 10^{-5}$  mbar, to conserve the cleanness of the surface.

### 4.2 ZrN Thin Films Synthesis

In this thesis work, the reactive d.c. magnetron sputtering deposition technique was applied to synthesize the zirconium nitride thin films. In the process, zirconium nitride thin films were deposited on clean silicon (100) substrates, from a highly pure Zr (99.5% purity) metallic target. Prior to deposition, the system was pumped down to a base pressure at about  $5 \times 10^{-6}$  mbar before Ar and N<sub>2</sub> gas are filled into the chamber. The argon inert gas was mixed into various ratios with nitrogen gas. The high negative voltage was then applied to the Zr target via the magnetron. If there is enough energy, both gases were ionized, and the ions of Ar<sup>+</sup> and N<sub>2</sub><sup>+</sup> were produced. The positive gas ions in plasma moved to bombard the target surface, following the electric field acceleration. This allowed the chemical reactions between surface atoms of the Zr target and colliding reactive gas happened, as illustrated in figure 4.1. The compound of ZrN is formed on few layers of target surface. This phenomenon is called “surface nitridation” [22]. Some of the Ar<sup>+</sup> and N<sub>2</sub><sup>+</sup> are accelerated and hit the target surface without compound reactions. ZrN atoms/clusters would be sputtered from the target surface, transport toward the substrate and the ZrN thin films are formed on the substrates via condensation. Note that,

in this thesis work, all the depositions were done at the ambient temperature, without using external substrate heating apparatus.

During sputtering process, secondary electrons are emitted from the target material at the same time. A magnetic field from the magnets behind the target (in the magnetron head) can be used to trap secondary electrons close to the target. The electrons follow helical paths around the magnetic field lines and impact with neutral gaseous near the target. This enhances the ionization of the plasma near the target leading to a higher sputter rate.

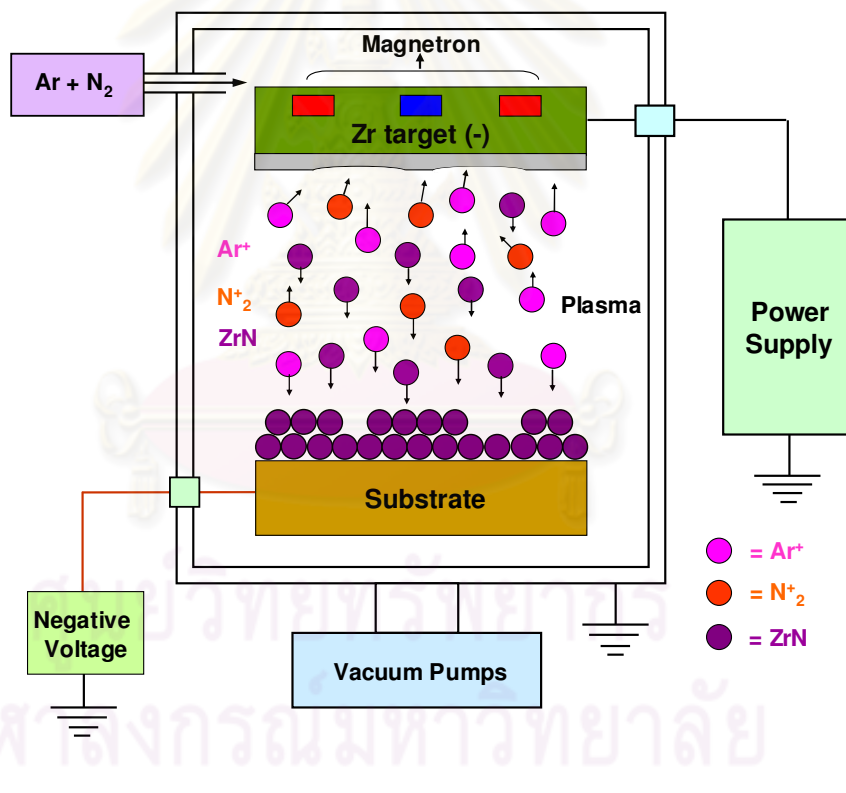


Figure 4.1: Schematic of ion-assisted reactive magnetron sputtering of zirconium nitride thin film

For ion-assisted sputter via substrate bias, a small negative voltage was applied to the substrate. It makes the positive ions such as Ar<sup>+</sup> and N<sub>2</sub><sup>+</sup> being accelerated to the

substrate. This will create many effects on the surface of the on-growing film material due to collisions. The maximum kinetic energy of ions moving to bombard the substrate can be determined from equation

$$E_i \approx e |V_s - V_p| \quad [\text{in unit of eV}] \quad (4.1)$$

where  $V_s$  is the negative substrate potential and  $V_p$  is the plasma potential [37].  $V_p$  can be obtained and calculated from plasma characterization measurement by using Langmuir probe measurement. For the system that we used in this work, the plasma potential was calculated to be 8 eV<sup>1</sup>. The energy of ions is proportional to the negative substrate potential, as the other parameters are constant for all samples. The energetically positive ions, especially N<sup>+</sup><sub>2</sub> ions can be occurred if there is energy greater than its molecule binding energy of 9.7 eV [38]. These ions will move to bombard the surface films. The energy and momentum of ions are then transferred to adatoms and some nuclei's. It makes the mobility of adatoms increased, and these adatoms move on surface to find the equilibrium lattice site [39]. Also, the ion bombardment on the film surface can make either the re-sputtering of the weakly bonded atoms and the atoms deeper into the films, especially in vacant sites. Therefore, the density of films can increase due to decreasing in void [40, 41].

### 4.3 Effects of the Nitrogen Partial Pressure

In this work, the nitrogen partial pressure and substrate bias voltage are the main variable in process. The first part was to find the optimum growth condition for film composition, effected by the nitrogen partial pressure. The base deposition condition is shown in table 4.1.

---

<sup>1</sup> P. Homhoul et al., Materials Transactions. (In manuscript)

|  |                            |
|--|----------------------------|
| Base pressure                                  | $5 \times 10^{-5}$ mbar    |
| Total working pressure ( Ar + N <sub>2</sub> ) | $4 \times 10^{-3}$ mbar    |
| The nitrogen partial pressure                  | varies with total pressure |
| Magnetron current                              | 0.80 A                     |
| Magnetron voltage                              | 350 V                      |
| Power consumption                              | 280 W                      |
| The distance between the target and substrate  | 12 cm                      |
| The substrate bias voltage                     | GND                        |

Table 4.1: Deposition conditions

From the EDS results, the ZrN thin films that grown with nitrogen partial pressure between 14-17% of total pressure, exhibit a stoichiometric composition, which show the yellow-gold color. The under-stoichiometric ZrN films (Zr-rich film) exhibits in the color as a silver metallic film and can be found from the films that grown at the nitrogen partial pressure less than 14%. While, the over-stoichiometric ZrN films (N-rich film) exhibits in the color of red or brown [9], [42] and can be found from the films that grown at the nitrogen partial pressure more than 17%. This is the similar appearance as in the case of TiN material [6].

The deposition rate decreases as the nitrogen partial pressure increase due to the target nitriding effects at the surface where the sputtering yield for nitride is much smaller than that for pure metal [9]. The N/Zr ratio also increases as an increasing of the nitrogen partial pressure due to the high nitrogen concentration incorporating into the film material. Thus, the nitrogen partial pressure in the process window that gives stoichiometric composition is only in between 14-17% of the total pressure, this is considered narrow. The deposition rate, chemical composition and color of the ZrN thin films as a function of nitrogen partial pressure can be summarized in table 4.2.

| $N_2$ (%) | Deposition rate (nm/min) | Zr (Atomic %) | $N_2$ (Atomic %) | $Zr_xN_y$         | Color                  |
|-----------|--------------------------|---------------|------------------|-------------------|------------------------|
| <14       | 24                       | 84.8          | 15.2             | $Zr_{1.3}N_{0.7}$ | Silver                 |
| 14-17     | 17                       | 54.8          | 45.2             | $Zr_{1.1}N_{0.9}$ | Yellow-gold            |
| >17       | 10                       | 24.8          | 75.2             | $Zr_{0.7}N_{1.3}$ | Red-gold, Brown, Black |

Table 4.2: The deposition rate, chemical composition and color of the ZrN thin films as a function of nitrogen partial pressure

The variation of color can be attributed to the increasing of  $N_2^+$  ion density in plasma. As the  $N_2^+$  ion density increases, more nitrogen can be incorporated and be deposited on the substrate surface [42]. The colors of the ZrN thin films are varied from silver to gold, red-gold, brown and black, just by varying nitrogen partial pressure, as shown in figure 4.2. A gold color was obtained only in the nitrogen partial pressure rang of 9.33% - 15.33% of total pressure. When the nitrogen partial pressure is more than 15.33% of total pressure, the surface color turns to red gold, brown and black [6, 42].

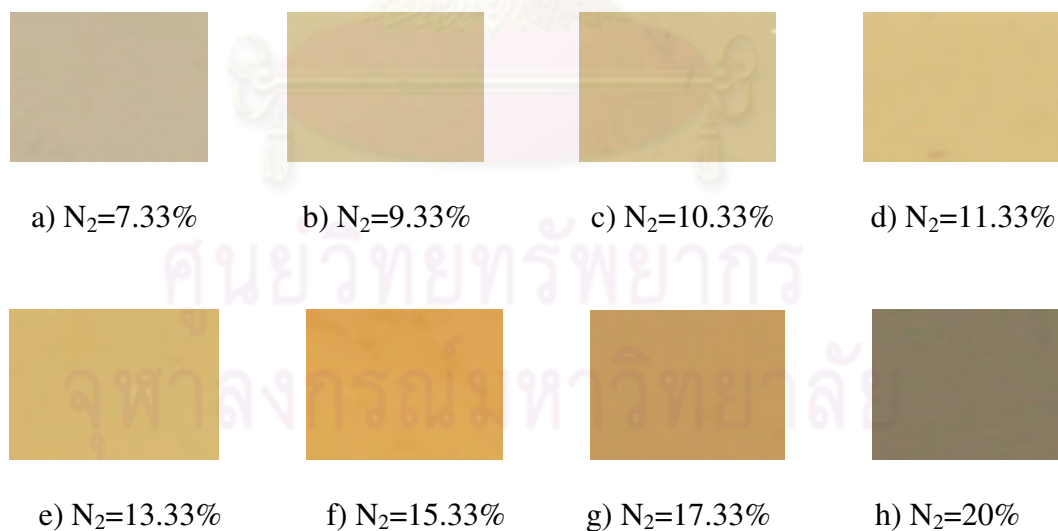


Figure 4.2: The colors of ZrN films deposited at nitrogen partial pressure of 7.33% (a), 9.33% (b), 10.33% (c), 11.33% (d), 13.33% (e), 15.33% (f), 17.33% (g) and 20% (h)

The summarized result from the x-ray diffraction of ZrN films is shown in figure 4.3. For under-stoichiometric ZrN films, the diffractogram of the film consists of two main textures, the (111) and (220). As nitrogen partial pressures increased, the stoichiometric composition of ZrN films can be obtained. The x-ray diffractogram of this ZrN thin film exhibited the (111), (200), (220) and (311) peaks. However, at more nitrogen partial pressure that gave an over-stoichiometry film, the peak of ZrN (200) and (311) disappeared. Note that, for all the specimens, the (111) is still a preferred orientation for all nitrogen partial pressures. Although, the (200) planes represent the most stable planes due to the minimum surface energy but the film that grow by d.c. sputtering usually has a highly surface mobility limitation [8, 9]. Therefore, the (111) with fast growth rate and low strain energy is dominate. Here, we can summarized that the nitrogen partial pressure in the process can be used to control the elemental composition of the film, the color appearance of the film and the crystal orientation of the films.

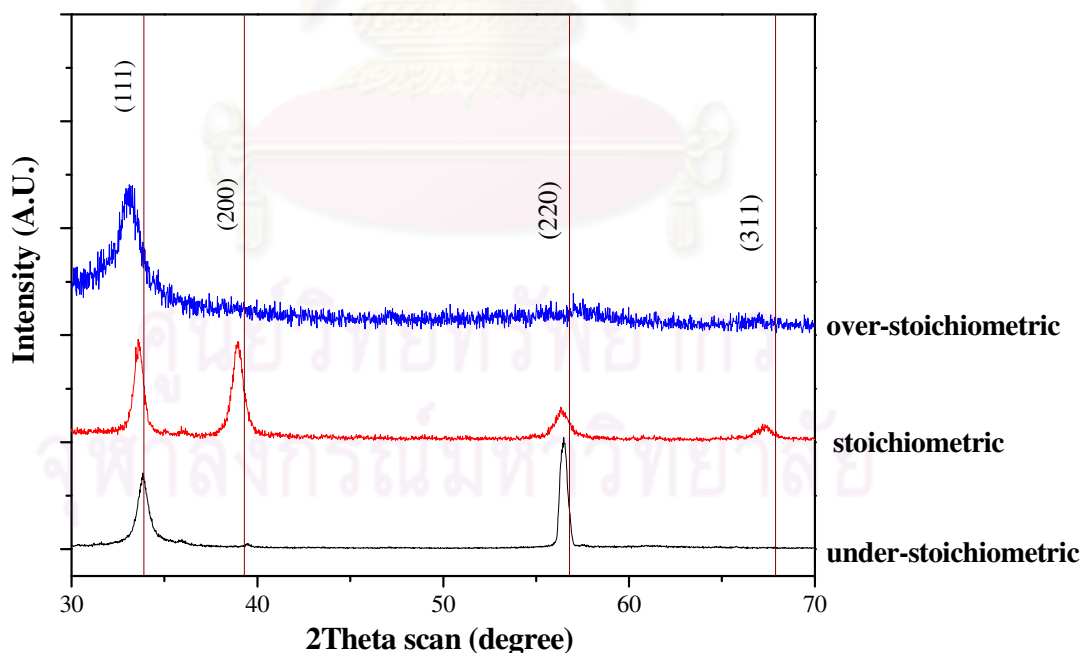


Figure 4.3: The X-ray diffraction patterns of the ZrN thin films with different stoichiometric

#### 4.4 Effects of Energetic Ions Assistance during Growth

From the previous experiment, we found the optimum growth condition for nitrogen partial pressure that gave a stoichiometric ZrN thin film material. This stoichiometric composition material can contribute to higher hardness value than the off-stoichiometric films due to crystallographic texture contained in the material [8]. In this part of the thesis, the ZrN thin films were still deposited on silicon (100) substrates, using the optimized nitrogen partial pressure condition from the previous part. In addition, the ion-assisted growth method via the substrate negative bias was also applied. The negative voltage was applied to the substrates from 0 V - 100 V during the growths. The effects of ion bombardment during thin film growth were investigated. As negative voltage is applied to the substrate, the positive ions such as  $\text{Ar}^+$  and  $\text{N}_2^+$  in the nearby plasma were accelerated toward the substrate, causing the bombardment. The maximum kinetic energy ( $E_i$ ) of ions, which is moving to bombard the substrate, can be approximately calculated from the equation (4.1). The plasma potential value, which obtained from the plasma characterization, was used in the calculation to determine the maximum kinetic energy of the bombarded ions. Deposition parameters that used in this experiment are summarized in Table 4.3.

|   |                         |
|---|-------------------------|
| Base pressure   | $5 \times 10^{-5}$ mbar |
| Total pressure ( Ar + N <sub>2</sub> )                          | $4 \times 10^{-3}$ mbar |
| The nitrogen partial pressure                                   | 17 % of total pressure  |
| Magnetron current   | 0.80 A                  |
| Magnetron voltage   | 350 V                   |
| Power consumption   | 280 W                   |
| The distance between the target and substrate                   | 12 cm                   |
| The substrate negative bias voltage                             | 0 V - 100 V             |
| The kinetic energy of ions (max)*<br>*(calculated from eq.4.1.) | 8 eV - 108 eV           |

Table 4.3: Deposition parameters

The elemental compositions of the ZrN thin films were measured by using EDS. The composition of the ZrN thin films, deposited at the nitrogen partial pressure 17% of total pressure and with different the energy of the assisted ions, were again investigated. As the substrate bias voltage was applied, the stoichiometric composition of the samples was slightly changed, while the color of samples remained the same. This can be summarized as in table 4.4.

| $V_s$ (V) | $E_i$ (eV) | Thickness (nm) | Zr (at. %) | $N_2$ (at. %) | $Zr_xN_y$         | Color       |
|-----------|------------|----------------|------------|---------------|-------------------|-------------|
| 0         | 8          | 974            | 51.1       | 48.9          | $Zr_{1.1}N_{0.9}$ | Yellow-gold |
| 30        | 38         | 893            | 51.5       | 48.5          | $Zr_{1.1}N_{0.9}$ | Yellow-gold |
| 50        | 58         | 848            | 49.3       | 50.7          | $Zr_{0.9}N_{1.1}$ | Yellow-gold |
| 75        | 83         | 344            | 48.5       | 51.5          | $Zr_{0.9}N_{1.1}$ | Yellow-gold |
| 100       | 108        | 204            | 49.4       | 50.6          | $Zr_{0.9}N_{1.1}$ | Yellow-gold |

Table 4.4: The chemical composition, color and thickness of ZrN thin films grown at the nitrogen partial pressure is 17% of total pressure with different the energy of ions

The contents of Zr in the ZrN films are fall in the range of 48.5%-51.5%, which still close to near stoichiometric form. The deposition rate, measured from the thickness change, is decreased as high energy of ions is used. This is due to the ions that are accelerated toward the substrate, have a large kinetic energy. This can induced high momentum impact on the on-growing film, leading to re-sputtering of the weakly bonded atoms and the decreasing of thickness [3, 14].

For the structural characterization, the comparison X-ray diffractographs of the stoichiometric ZrN thin films grown at different the energy of assisted ions, are shown in figure 4.4. The ZrN thin films still exhibited NaCl cubic structure pattern with the orientation peaks of (111), (200), (220) and (311), respectively. The (111), (200), (220) and (311) correspond to the  $2\theta$  angles at  $33.9^\circ$ ,  $39.3^\circ$ ,  $56.8^\circ$  and  $67.9^\circ$ , respectively. As the energy of the assisted ions change, there are some slightly change in the peak-intensity ratio. The ZrN (311) slightly disappears as high energy of ions was applied. The

(111) peak is still remain a preferred orientation for all the growths. However, with energy of ions at 38 eV, this results in the most development of (220) from ion-assisted growth. For the normal case of the fourth group of transition metals nitride material, the (200) is the most stable planes with the minimum surface energy while the growth of (111) is controlled by the strain energy [43]. Although, the (200) represent the most stable planes, the (220) is also playing roles in the hardness contribution [8, 9].

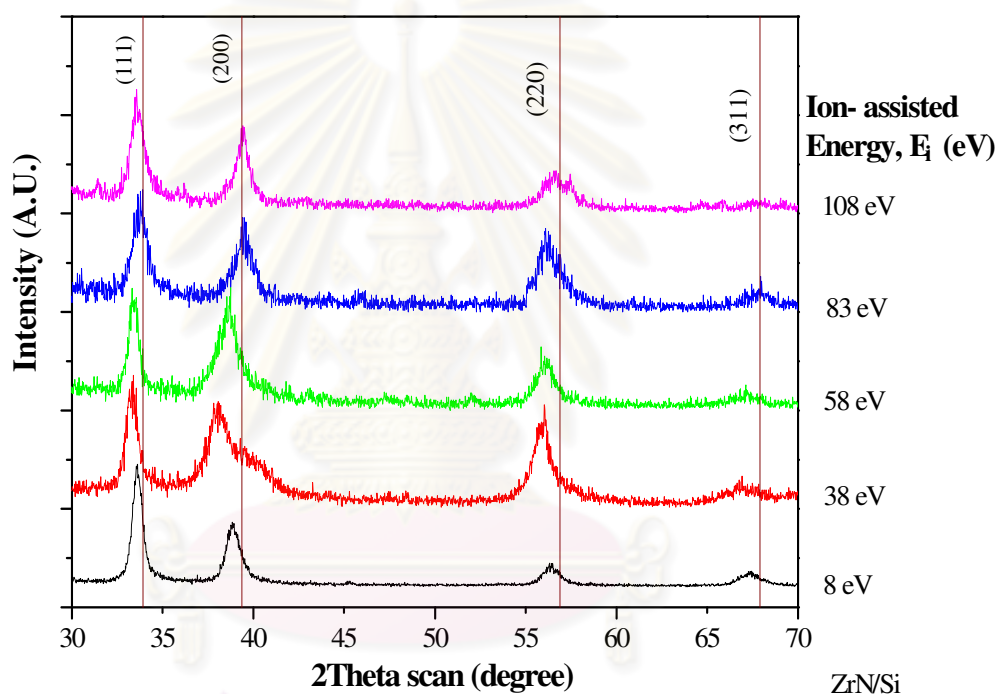


Figure 4.4: The X-ray diffraction patterns of the stoichiometric ZrN thin films grown with different the energy of assisted ions

The surface morphology of ZrN thin films was investigated by atomic force microscope (AFM). The maximum root-mean-square roughness (RMS) is at 1.96 nm for the ZrN thin film grown with assisted-ions at energy of about 8 eV. The RMS roughness decreases down to 0.51 nm as energy of assisted ion increase up to 108 eV, as illustrated in figure 4.5. The root-mean-square surface roughness tends to decrease as high substrate bias voltage is applied. This is because, at higher substrate bias voltage, the energetic

ions, which are accelerated by electric field toward the substrate, have higher energy induced an increasing in surface mobility of adatoms. This can help to move the adatoms on surface to find the equilibrium lattice site. This can also result in a suppression of the 3-D island growth mechanism in the low growth temperature regime [14, 39]. Thus, the surface morphology of the ZrN films depends on the energy of ions which can be controlled and optimized.

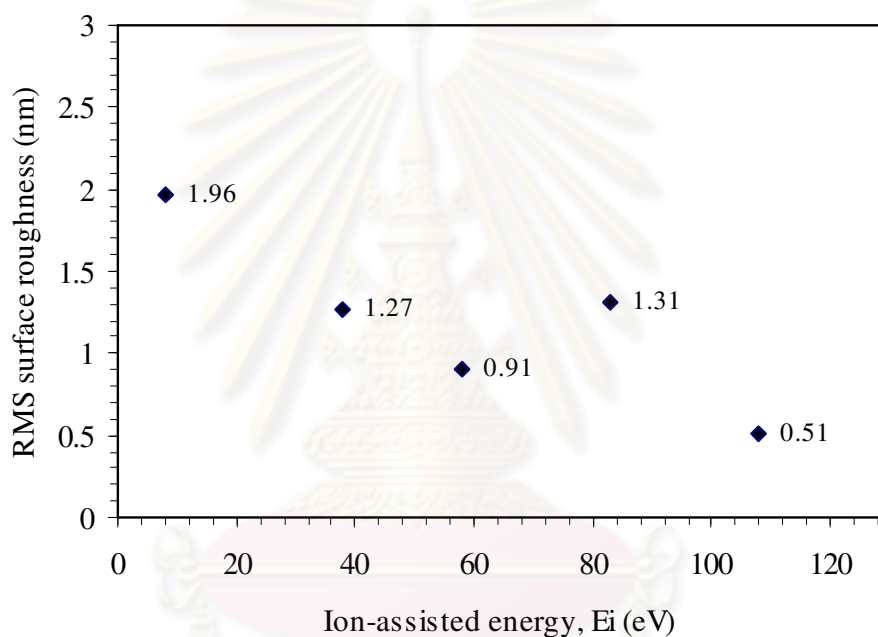


Figure 4.5: RMS surface roughness of the stoichiometric ZrN thin films grown with different the energy of assisted ions

At zero bias (8 eV), the mobility of the adatoms is still quite low and the surface mobility is limited. Increasing substrate bias, the energy of the assisted ions also increases, thereby enhancing mobility of the adatoms and suppression the island or facet growth [14]. This can reduce down the roughness of the surface morphology, as illustrated in figure 4.6. (a)-(e).

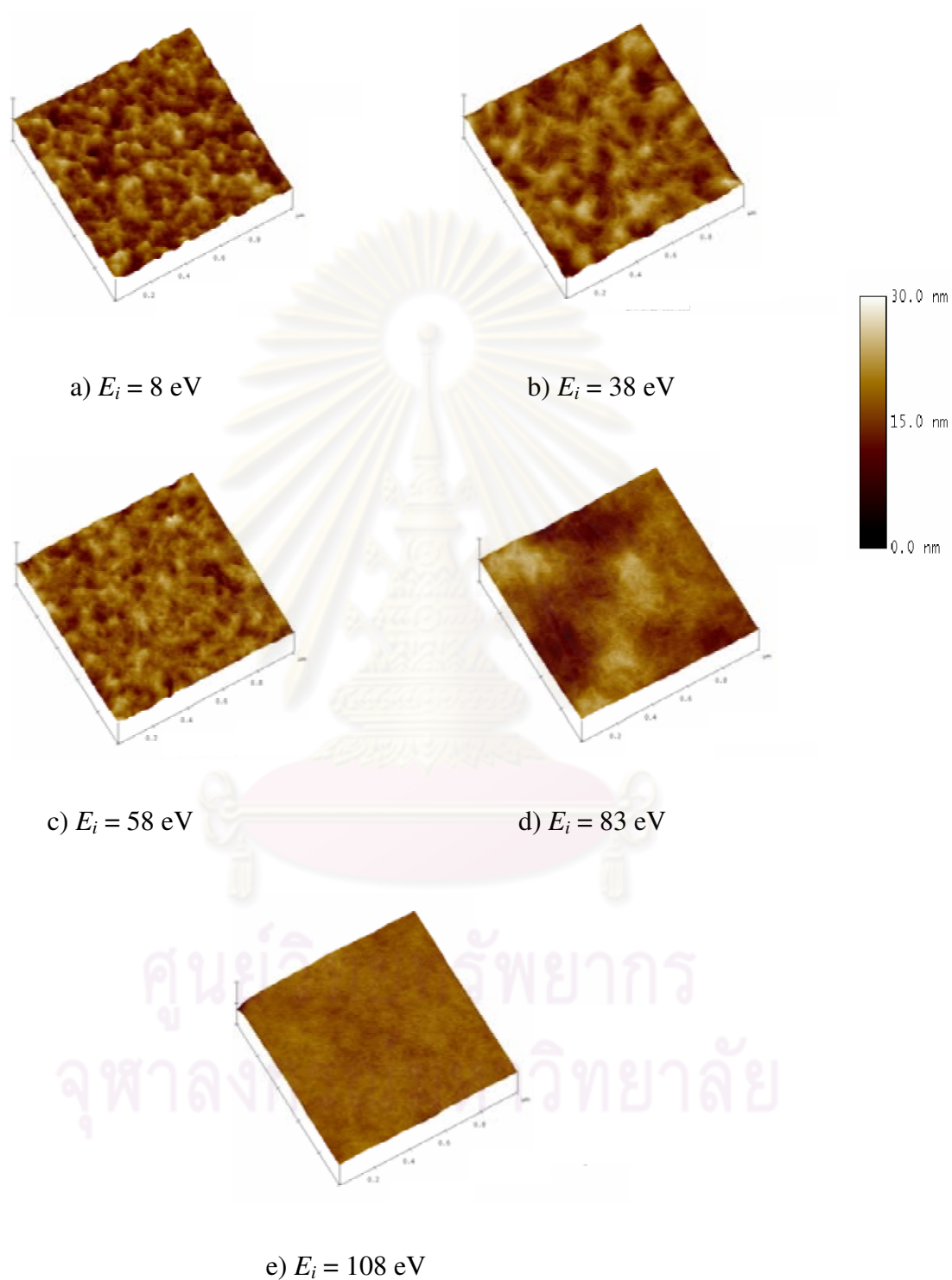


Figure 4.6: The AFM images of ZrN films deposited with assisted ions at energy of 8 eV (a), 38 eV (b), 58 eV (c), 83 eV (d) and 108 eV (e), respectively. (Data scale 30 nm)

For mechanical properties, the CSM™ nanoindenter is used to determine the hardness of the ZrN thin films. A Berkovich-type diamond indenter tip is used. In the measurements, the maximum indenter depth penetration was kept less than 10% of the film thickness to prevent the substrate effects. For ZrN thin films, the maximum value of hardness is at 38.7 GPa for the film grown with the energy ions of 38 eV, as shown in figure 4.7.

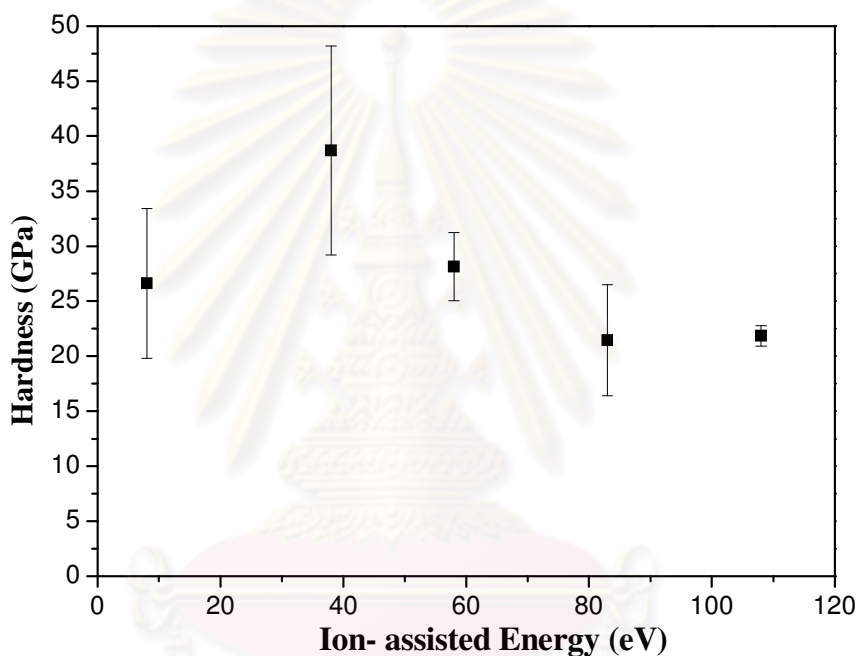


Figure 4.7: The hardness of stoichiometric ZrN thin films grown with different the energy of assisted ions

Compare to the film grown without substrate bias, the use of low-energy ion-assisted growth of ZrN can improve the hardness of the material up to about 45%. This can consider to a longer lifetime for the coated applications. At low-energy ion bombardment, the ions nearby the substrate move to bombard the film surface and induce an increasing of the denseness of the films by an increasing of the surface diffusion [14]. For higher ion energies ( $E_i > 38\text{eV}$ ), the accelerated ions have a larger kinetic energy and cause higher momentum impact on the on-growing films. This leads to re-sputtering of the weakly bonded atoms, which can effect on the mechanical properties of the films. Also,

this can reduce the deposition rate [3]. However, this can reduce the roughness of film surface, as indicated from the AFM results.

#### 4.5 Effects of the Post-Annealing and Metallic Interlayer

The thermal stability and decomposition test are made in this point. As-deposited ZrN thin films from previous part were annealed at 350°C for 60 min in Ar, with the ramping rate at 1°C/min. After annealing, the elemental compositions of the ZrN thin films were measured by using EDS. The ZrN thin films still exhibit stoichiometric composition for all samples, as summarized in table 4.5. The color of the ZrN thin film did not change and the oxygen contents was not found in the films after annealing. This result indicates that the ZrN thin films have exhibited a good thermal stability at this temperature [20].

| $E_i$ (eV) | Zr (at. %) | N <sub>2</sub> (at. %) | Zr <sub>x</sub> N <sub>y</sub>     | Color       |
|------------|------------|------------------------|------------------------------------|-------------|
| 8          | 49.2       | 51.8                   | Zr <sub>0.9</sub> N <sub>1.1</sub> | Yellow-gold |
| 38         | 46.9       | 53.1                   | Zr <sub>0.9</sub> N <sub>1.1</sub> | Yellow-gold |
| 58         | 44.8       | 55.2                   | Zr <sub>0.9</sub> N <sub>1.1</sub> | Yellow-gold |
| 83         | 48.7       | 51.3                   | Zr <sub>0.9</sub> N <sub>1.1</sub> | Yellow-gold |
| 108        | 45.2       | 54.8                   | Zr <sub>0.9</sub> N <sub>1.1</sub> | Yellow-gold |

Table 4.5: The elemental compositions and color of ZrN thin films after annealing

The surface morphology of thin films is observed by SEM, the ZrN thin films that grown directly on Si (100) substrate exhibited de-lamination and discontinuity of the film surface. This can be due to a large different in thermal expansion coefficient between ZrN thin film and Si substrate [45] ( $\alpha_{ZrN} = 7.24 \times 10^{-6} \text{ K}^{-1}$ ,  $\alpha_{Si} = 2.33 \times 10^{-6} \text{ K}^{-1}$  and  $\alpha_{Zr} = 5.7 \times 10^{-6} \text{ K}^{-1}$ ) [2, 46]. Here, we introduced the zirconium metallic interlayer about 500 nm thick between ZrN film and Si substrate. This film structure of ZrN/Zr exhibited continuity of the surface without de-lamination or peel off. This indicates that the Zr interlayer between ZrN and Si (100) substrate can help to improve film adhesion [44], as shown in figure 4.8.

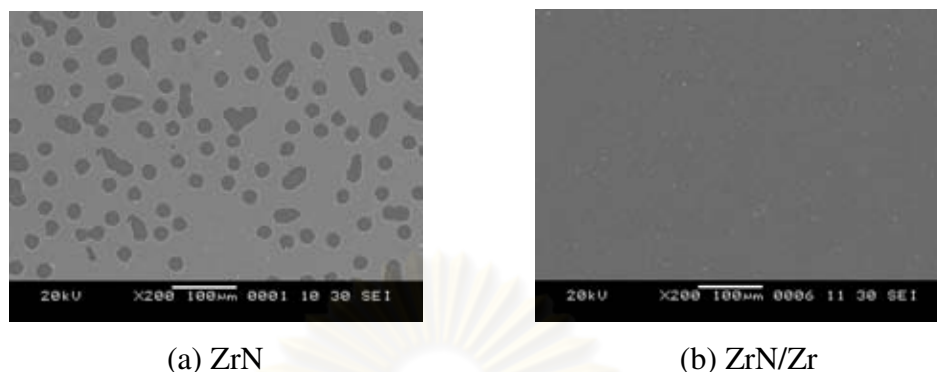


Figure 4.8 The SEM images of ZrN and ZrN/Zr films after annealing at 350°C

For the structural characterization, it can be seen that cubic ZrN phase is present in all the samples. The XRD intensity of ZrN thin film is slightly changed and the oxide diffraction peaks cannot be discerned with the annealing, as shown in figure 4.9.

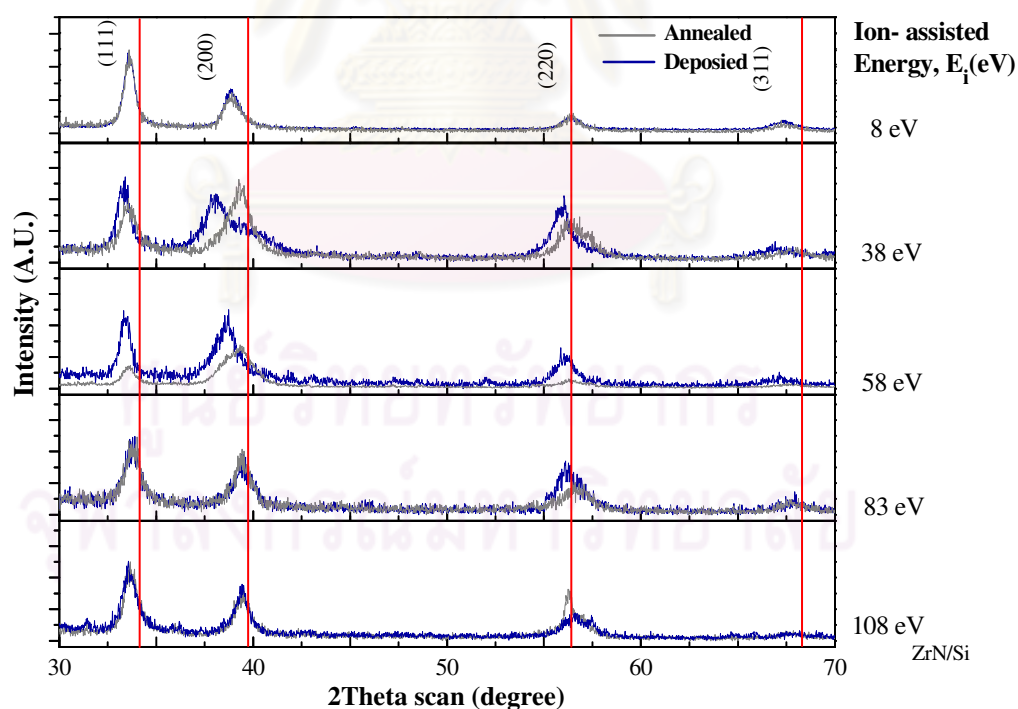


Figure 4.9: XRD patterns of zirconium nitride thin films grown at different the energy of assisted ions, before and after annealing at 350°C for 60 min

Therefore, the thermal treatment at this temperature does not critically affect the crystalline structure of ZrN. The result for the case of ZrN/Zr thin films is also quite similar. The slightly shift in the peak position can be due to the relaxation of the crystal lattice metric in the film after annealing [20].

After annealing, ZrN thin films do not show a significant change in the hardness values, which are shown in figure 4.10. This result indicates that Zr interlayer does not influence to the hardness but Zr interlayer between ZrN and Si substrate can improve interface adhesion of ZrN/Zr with a Zr interlayer may be attributed to the decrease of residual stress [44].

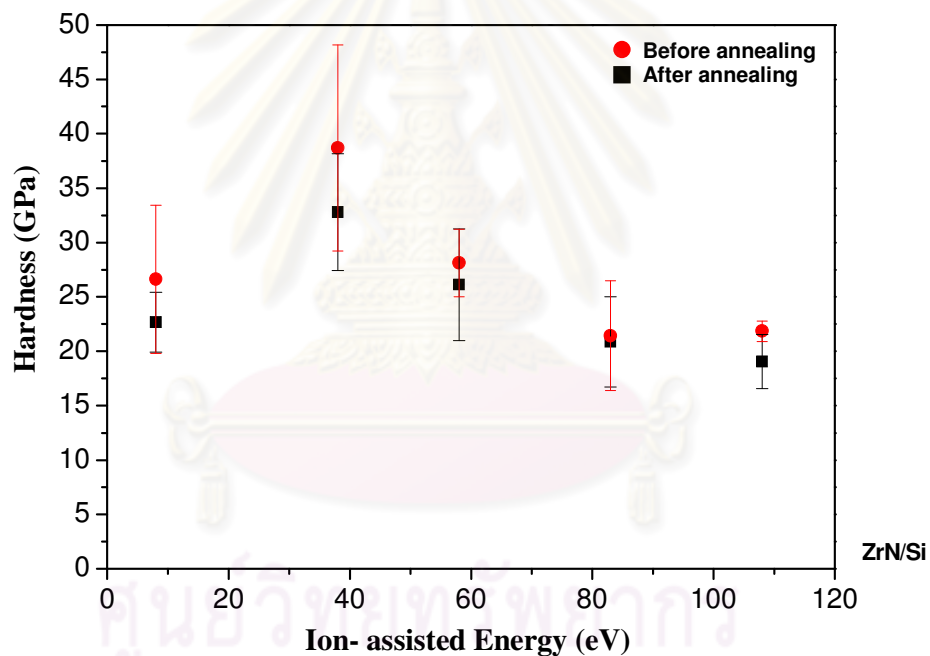


Figure 4.10: The hardness of ZrN thin films grown at different the energy of assisted ions, before and after annealing at 350°C for 60 min ZrN

# CHAPTER V

## SUMMARY AND CONCLUSIONS

Zirconium nitride (ZrN) thin films were synthesized and deposited on silicon (100) substrates by ion-assisted reactive d.c. magnetron sputtering in a mixture of Ar-N<sub>2</sub> atmosphere. In this thesis work, we have investigated for the optimized condition of main key process parameters of ZrN thin film, such as nitrogen partial pressure and energy of the assisted ions. We have also characterized the properties of ZrN thin films and the improvement of their properties.

For the optimization on the nitrogen partial pressure, the nitrogen partial pressure that can give the stoichiometric composition ZrN film is in the range between 14-17% for the low temperature growth regime. The stoichiometric composition is also can be noticed from the color of the film, which is bright yellow-gold [6]. The nitrogen partial pressure has a significant effect on the elemental composition of material, the deposition rate, crystal preferred orientation and color of the films. For the decorative coating applications, this is a key factor for color selection of the coated surface. The crystal structures of the films were characterized by using XRD. The film structure exhibited the orientations of (111), (200), (220) and (311), in the texture competitive growth mode. For stoichiometric composition ZrN film, the diffractograph shows the ZrN (200) planes, which represent the most stable planes. This contributes to the hardness of the film.

We have investigated the variation of the energy of the assisted-ions ( $E_i$ ) during growth, while the flow rate of Ar and N<sub>2</sub> was kept constant at the optimized condition. The use of assisted-ions made just a slightly change in the composition. On the others hand, the low energy ion bombardment can promote an increase in the hardness and smoothness of the film surface. Both root-mean-square surface roughness and the hardness are affected by the ions moving to bombard the surface films, and then the energy and momentum of ions are transferred to adatoms. It makes an increase in mobility of adatoms and suppression the 3D island growth mode [39]. The highest

hardness for ZrN (38.7 GPa) can be obtained from the stoichiometric film grown with the energy of assisted ion at 38 eV. At this low-energy ion bombardment, the ions nearby the substrate moved to bombard the surface films and induce an increasing of the denseness of the films by an increasing of the surface diffusion of adatoms.

After annealing at 350°C for 60 min, The ZrN thin films still exhibit stoichiometric composition for all samples. The hardness value is slightly decreased but not significant. Not only the color of the ZrN thin film didn't change but also the oxygen could not be found in the films. This result indicates quite good thermal stability of the ZrN thin films. However, the de-lamination and peel off can be observed due to the different in thermal expansion coefficient between film and substrate. This aspect can be solved by introduce the Zr metallic interlayer between ZrN film and Si substrate. This Zr interlayer can promote the adhesion between film and substrate without disturbing the hardness and composition [44].

## References

- [1] D. Pilloud, J.F. Pierson, A. Cavaleiro and M.C. Marco de Lucas. Effect of germanium addition on the properties of reactively sputtered ZrN films. *Thin Solid Films*. 492 (2005): 180-186.
- [2] Wen-Jun Chou, Ge-Ping Yu and Jia-Hong Huang. Bias effect of ion-plated zirconium nitride film on Si (100). *Thin Solid Films*. 405 (2002):162-169.
- [3] D. Pilloud, A.S. Dehlinger, J.F. Pierson, A. Roman and L. Pichon. Reactively sputtered zirconium nitride coatings: structural, mechanical, optical and electrical characteristics. *Surf. Coat. Technol.* 174-175 (2003): 338-344.
- [4] Jia-Hong Huang, Chi-Hsin Ho and Ge-Ping Yu. Effect of nitrogen flow rate on the structure and mechanical properties of ZrN thin films on Si (1 0 0) and stainless steel substrates. *Mater. Chem. Phys.* 102 (2007): 31-38.
- [5] D.F. Arias, Y.C. Arango and A. Devia. Study of TiN and ZrN thin films grown by cathodic arc technique. *Appl. Surf. Sci.* 253 (2006): 1683-1690.
- [6] M. Nose, M. Zhou, E. Honbo, M. Yokota and S. Saji. Colorimetric properties of ZrN and TiN coatings prepared by DC reactive sputtering. *Surf. Coat. Technol.* 142-144 (2001): 211-217.
- [7] Henry J. Ramos and Nicomedes B. Valmoria. Thin film deposition of ZrN using plasma sputter type negative ion source. *Vacuum*. 73 (2004): 549- 554.
- [8] M.M. Larijani, N. Tabrizi, Sh. Norouziana, A. Jafari, S. Lahouti, H. Haj Hosseini and N. Afshari. Structural and mechanical properties of ZrN films prepared by ion beam sputtering with varying N<sub>2</sub>/Ar ratio and substrate temperature. *Vacuum*. 81 (2006): 550-555.
- [9] Chuan-Pu Liu and Heng-Ghieh Yang. Systematic study of the evolution of texture and electrical properties of ZrN<sub>x</sub> thin films by reactive DC magnetron sputtering. *Thin Solid Films*. 444 (2003): 111-119.

- [10] Jia-Hong Huang, Hao-Chung Yang, Xing-Jian Guo and Ge-Ping Yu. Effect of film thickness on the structure and properties of nanocrystalline ZrN thin films produced by ion plating. *Surf. Coat. Technol.* 195 (2005): 204-213.
- [11] M. Del Re, R.Gouttebaron, J.-P. Dauchot, P. Leclere, G. Terwagne and M. Hecq. Study of ZrN layers deposited by reactive magnetron sputtering. *Surf. Coat. Technol.* 174-175 (2003): 240-245.
- [12] H.M. Benia, M. Guemmaz, G. Schmerber, A. Mosser and J.-C. Parlebas. Investigations on non-stoichiometric zirconium nitrides. *Appl. Surf. Sci.* 200 (2000): 231-238.
- [13] H.M. Benia, M. Guemmaz, G. Schmerber, A. Mosser and J.C. Parlebas. Optical properties of non-stoichiometric sputtered zirconium nitride films. *Appl. Surf. Sci.* 211 (2003): 146-155.
- [14] E.W. Niu, L. Li, G.H. Lv, H. Chen, W.R. Feng, S.H. Fan, S.Z. Yang and X.Z. Yang. Influence of substrate bias on the structure and properties of ZrN films deposited by cathodic vacuum arc. *Mater. Sci. Eng.* 460-461 (2007): 135-139.
- [15] Cheng-Shi Chen, Chuan-Pu Liu, C.-Y.A. Tsao and Heng-Ghieh Yang. Study of mechanical properties of PVD ZrN films, deposited under positive and negative substrate bias conditions. *Scripta Mater.* 51 (2004): 715-719.
- [16] Ausis. *File: Nacl-structure. jpg*. [online]. 2009. Available form: [http://commons.wikimedia.org/wiki/Image: Nacl-structure. jpg](http://commons.wikimedia.org/wiki/Image:Nacl-structure.jpg) [2009, Jan 26]
- [17] J.V. Ramana, Sanjiv Kumar, Christopher David, A.K. Ray and V.S. Rajub. Characterisation of zirconium nitride coatings prepared by DC magnetron sputtering. *Mater. Lett.* 43 (2000): 73-76.
- [18] Chuan-Pu Liu and Heng-Ghieh Yang. Deposition temperature and thickness effects on the characteristics of d.c. sputtered ZrN<sub>x</sub> films. *Mater. Chem. Phys.* 86 (2004): 370-374.
- [19] H.M. Benia, M. Guemmaz, G. Schmerber, A. Mosser and J.C. Parlebas. Optical and electrical properties of sputtered ZrN compounds. *Catal. Today.* 89 (2004): 307-312.

- [20] M.A. Auger, J.J. Araizab, C. Falcony, O.Sanchez and J.M. Albella. Hardness and tribology measurements on ZrN coatings deposited by reactive sputtering technique. *Vacuum*. 81 (2007): 1462- 465.
- [21] Lili Hu, Dejie Li and Guojia Fang. Influence of N<sub>2</sub>: (N<sub>2</sub> + Ar) flow ratio and substrate temperature on the properties of zirconium nitride films prepared by reactive d.c. magnetron sputtering. *Appl. Surf. Sci.* 220 (2003): 367-371.
- [22] David, A.G. and Ismat S. *Handbook of Thin Film Process technology*. Philadelphia: Institute of Physics Publishing, 1996.
- [23] Ohring, M. *The materials science of thin films*. San Diego: Academic Press, 1992.
- [24] Sukkaneste T. *Growth of Wide- band Gap AlN And (SiC)<sub>x</sub>(AlN)<sub>1-x</sub> Thin Films by Reactive Magnetron Sputter Deposition*. Doctoral Dissertation, Department of Physics and Measurement Technology, Linkoping University, 2001.
- [25] Chapman, B. *Glow discharge process: Sputtering and plasma etching*. New York: John Wiley and Sons, 1980.
- [26] David Ross Mcgregor JR. *Growth Optimization and Characterization of Reactively Sputtered Zirconium Nitride Thin Films for III-V Buffer Layer Applications*. Master's Thesis, Department of Materials Science and Engineering, North Carolina State University, 2002.
- [27] P.J. Goodhew. *Electron microscopy and analysis*. London and Winchester: Wykeham publication (London) LDT, 1975.
- [28] Darrell Henry. *Electron – sample interactions* [online]. 2007. Available from: [http://serc.carleton.edu/research\\_education/geochemsheets/electroninteractions.html](http://serc.carleton.edu/research_education/geochemsheets/electroninteractions.html). [2010, Jan 4]
- [29] Stanley L. Flegler, Jonh W. Heckman, Jr. And Karen L. Klomparens. *Scanning and transmission electron microscopy an introduction*. New York: Oxford University Press, 1995.
- [30] Wikipedia. *Energy-dispersive X-ray spectroscopy* [online]. 2009. Available from: [http://en.wikipedia.org/wiki/Energy\\_dispersive\\_X-ray\\_spectroscopy](http://en.wikipedia.org/wiki/Energy_dispersive_X-ray_spectroscopy). [2010, Jan 4]

- [31] Wikipedia. *Atomic force microscope block diagram. svg*. [online]. 2009. Available from:[http://en.wikipedia.org/wiki/File:Atomic\\_force\\_microscope\\_block\\_diagram.svg](http://en.wikipedia.org/wiki/File:Atomic_force_microscope_block_diagram.svg). [2010, Jan 4]
- [32] Ferdinand Walther, Wolfgang M. Heckl and Robert W. Stark. Evaluation of nanoscale roughness measurements on a plasma treated SU-8 polymer surface by atomic force microscopy. *Appl. Surf. Sci.* 254 (2008): 7290-7295.
- [33] Anthony C. Fischer-Cripps. *Mechanical engineering series nanoindentation*. New York: Springer-Verlag New York, LLC, 2004.
- [34] Dehong Huo, Yingchun Liang and Kai Cheng. An investigation of nanoindentation tests on the single crystal copper thin film via an AFM and MD simulation. *Journal of Mechanical Engineering Science* 221 (2007): 259-266.
- [35] Chingfu Tsou, Changchun Hsu and Weileun Fang. Interfaces friction effect of sliding contact on nanoindentation test. *Sens. Actuators A*. 117 (2005): 309-316.
- [36] D. Beegan, S. Chowdhury and M.T. Laugier. Comparison between nanoindentation and scratch test hardness (scratch hardness) values of copper thin films on oxidised silicon substrates. *Surf. Coat. Technol.* 201 (2007): 5804-5808.
- [37] C.-S. Shin, D. Gall, Y.-W. Kim, N. Hellgren, I. Petro, and J.E. Greene. Development of Preferred Orientation in Polycrystalline NaCl-structure  $\delta$ -TaN Layers Grown by Reactive Magnetron Sputtering: Role of Low-Energy Ion/Surface Interactions. *J. Appl. Phys.* 92, (2002): 5084.
- [38] L. Hulman, U. Helmersson, S.A. Barnett, J.E. Sundgren and J.E. Greene. Low-energy ion irradiation during film growth for reducing defect densities in epitaxial TiN(100) films deposited by reactive-magnetron sputtering. *J. Appl. Phys.* 61 (1987) 552-555.
- [39] J.-H. Huang, K.-W. Lau and G.-P. Yu. Effect of nitrogen flow rate on structure and properties of nanocrystalline TiN thin films produced by unbalanced magnetron sputtering. *Surf. Coat. Technol.* 191 (2005): 17-24.

- [40] S. Logothetidis, I. Alexandrou and S. Kokkou. Optimisation of TiN thin film growth with in situ monitoring: The effect of bias voltage and nitrogen flow rate. *Surf. Coat. Technol.* 80 (1996): 66-71.
- [41] P.-K. Huang and J.-W. Yeh. Effects of substrate bias on structure and mechanical properties of (AlCrNbSiTiV)N coatings. *J. Phys. D: Appl. Phys.* 42 (2009): 115401.
- [42] Zhang Zhiguo, Liu Tianwei, Xu Jun, Deng Xinlu and Dong Chuang. N-rich Zr-N films deposited by unbalanced magnetron sputtering enhanced with a highly reactive MW-ECR plasma. *Surf. Coat. Technol.* 200 (2006): 4918-4922.
- [43] Yu-Chih Chieh, Wen-Zheng Lo and Fu-Hsing Lu. Microstructure evolution of ZrN films annealed in vacuum. *Surf. Coat. Technol.* 200 (2006): 3336-3340.
- [44] Deng Jianxin, Liu Jianhua, Zhao Jinlong, and Song Wenlong. Wear mechanisms of PVD ZrN coated tools in machining. *Int J Refract Met Hard Mater.* 26 (2008): 164-172.
- [45] J.-H. Huang, C.-Y. Hsu, S.-S. Chen and G.-P. Yu. Effect of substrate bias on the structure and properties of ion-plated ZrN on Si and stainless steel substrates. *Mater. Chem. Phys.* 77 (2002): 14-21.
- [46] The university of Sheffield and WebElements Ltd, UK. *Zirconium: physical properties* [online]. 1993. Available from: <http://www.webelements.com/zirconium/physics.html>. [2010, Jan 26]



## **Appendices**

ศูนย์วิจัยทรัพยากร  
จุฬาลงกรณ์มหาวิทยาลัย

## Appendix A

### Conference Presentations

1. **Jirawan Saenton**, Sakuntam Sanorpim, Surasing Chaiyakhun and Sukkaneste Tungasmita. Structural Characterization of Zirconium Nitride (ZrN) Films Grown by Reactive DC Magnetron Sputtering. *35<sup>th</sup> Congress on Science and Technology of Thailand (STT.35)*, Bang-Saen, Chonburi, Thailand 15-17 October, 2009 (**Poster presentation**).
2. **Jirawan Saenton**, Sakuntam Sanorpim, Surasing Chaiyakhun and Sukkaneste Tungasmita. Ion-assisted Growth of Zirconium Nitride (ZrN) Thin Films Deposited by Reactive DC Magnetron Sputtering. *7<sup>th</sup> Eco-Energy and Materials Science and Engineering Symposium (7<sup>th</sup> EMSES)*, Chiang Mai, Thailand 17-20 November, 2009 (**Oral presentation**).

ศูนย์วิทยทรัพยากร  
จุฬาลงกรณ์มหาวิทยาลัย

# Appendix B

## Proceeding

Print Main Menu

Close Paper

7th Eco-Energy and Materials Science and Engineering Symposium, Chiang Mai, Thailand 19-22 Nov. 2009

### Ion-assisted Growth of Zirconium Nitride (ZrN) Thin Films Deposited by Reactive DC Magnetron Sputtering

J. Saenton, S. Sanorpim, S. Chaiyakhun and S. Tungasmita\*

**Abstract** Zirconium nitride (ZrN) thin films were deposited on the silicon (100) substrates by reactive dc magnetron sputtering in a mixture of Ar-N<sub>2</sub> atmosphere. In this work, we investigated the effect of nitrogen partial pressures and ion bombardment on the surface of on-growing films by substrate bias voltage, toward the properties of ZrN thin film. The elemental composition of the films was investigated by using energy dispersive spectroscopy (EDS). For optimized condition of the stoichiometric ZrN film, the nitrogen partial pressure in the process window was found in the range between 17-18% of the total pressure, which is considered narrow. The high nitrogen partial can cause a decreasing in deposition rate due to the poisoning effect. The crystal structures of the films were characterized by using x-ray diffraction (XRD). The films exhibited the texture competitive development of (111), (200), (220) and (311). The surface roughness decrease with the increase of substrate bias voltage: kinetic energy of impact ions,  $E_i$ . The maximum hardness value was found at 38.69 GPa for the film grown with  $E_i=38$  eV.

**Keywords** ZrN, sputtering, thin film, ion-surface interactions.

#### 1. INTRODUCTION

Transition metal nitrides films are widely used as diffusion barriers in microelectronics, hard coatings on cutting tools or as corrosion and abrasion resistant layers on optical and mechanical components. Among the different transition metal nitrides (TiN, CrN, HfN, TaN, etc.) zirconium nitride (ZrN) is another attractive material due to its good chemical and physical properties [1] such as high hardness (up to 40 GPa, approximately) [2], low electrical resistivity, high chemical and thermal stability [3], warmer golden color, corrosion resistance [4], low friction coefficient, high melting point and biocompatibility [5]. This makes zirconium nitride has been used in many application such as cutting tools for enhance the lifespan of the tools, medical tools, optical application for heat mirrors [6], diffusion barriers in semi-conductor technology, cryogenic thermometer [7] and decorative coating because of their high chemical stability and scratch resistance.

In this work, the reactive d.c. magnetron sputtering technique is used for synthesis ZrN thin films. The nitrogen partial pressure and substrate bias voltage are focused growth parameters in process. The aim of this work is to investigate the influence of those growth parameters on the chemical composition, structure,

morphology and mechanical properties of ZrN thin films.

#### 2. EXPERIMENTAL PROCEDURES

The Zirconium nitride (ZrN) thin films were deposited on silicon (100) substrates using Zr (99.5% purity) target by ion-assisted reactive dc magnetron sputtering. Prior to the deposition process, the specimens were chemically cleaned in trichloroethylene acetone, methanol, and then blown dried with dry N<sub>2</sub>, respectively. The chamber was evacuated to a base pressure of  $5 \times 10^{-5}$  mbar. The nitrogen partial pressures were varied while the total pressure (Ar+N<sub>2</sub>) was fixed at  $4 \times 10^{-3}$  mbar. In this work, the distance between the target and the substrates is also fixed at 12 cm. A constant current of 0.8 A is applied to the target and the pre-sputtered was done for 5 min. A negative bias voltage ranging from 0 V to 100 V was applied to the substrate. The depositions were done at the ambient temperature, without using external substrate heating apparatus. The crystal structure of films was analyzed by Bruker D8 x-ray diffraction (XRD). The surface morphology and roughness of films were determined by the JEOL JSM-6480LV scanning electron microscope (SEM) and Veeco Nanoscope - IV atomic force microscopy (AFM). The chemical composition of the films was characterized by Oxford's INCA energy dispersive spectroscopy (EDS). The hardness of the films was measured by using CSM™ Berkovich diamond tip nanoindenter.

In bias sputtering process, a negative voltage is applied to the substrate. This makes the positive ions such as Ar<sup>+</sup> and N<sup>+</sup> in the plasma were accelerated toward the substrate, causing the bombardment. The maximum kinetic energy ( $E_i$ ) of ions moving to bombard the substrate can be approximately calculated as the below equation [8].

$$E_i = e |V_s - V_b| \quad [\text{in the unit of eV}] \quad (1)$$

J. Saenton is with the Department of Physics, Faculty of Science Chulalongkorn University, Payathai Road, Wangmai, Pathumwan, Bangkok 10330, Thailand, E-mail: [jss@physics.chula.ac.th](mailto:jss@physics.chula.ac.th)

S. Sanorpim is with the Department of Physics, Faculty of Science Chulalongkorn University, Payathai Road, Wangmai, Pathumwan, Bangkok 10330, Thailand, E-mail: [ssanorpim@chula.ac.th](mailto:ssanorpim@chula.ac.th)

S. Chaiyakhun is with the Department of Physics, Faculty of Science Burapha University, Bangsuea, Choburi 20131, Thailand, E-mail: [s-chaiyakhun@bu.ac.th](mailto:s-chaiyakhun@bu.ac.th)

S. Tungasmita is with the Department of Physics, Faculty of Science Chulalongkorn University, Payathai Road, Wangmai, Pathumwan, Bangkok 10330, Thailand, E-mail: [sukkoneste.t@chula.ac.th](mailto:sukkoneste.t@chula.ac.th)

(\* corresponding author)

where  $V_s$  is the negative substrate voltage.

$V_p$  is the plasma potential.

### 3. RESULTS AND DISCUSSION

#### 3.1 Nitrogen Partial Pressure

The deposition rate, chemical composition and color of the ZrN thin films are shown in table 1. The deposition rate decrease as the nitrogen partial pressure increase due to the target nitriding effects at the surface where the sputtering yield for nitride is much smaller than the metal [9]. The N/Zr ratio increases as an increasing of the nitrogen partial pressure due to the high nitrogen concentration incorporate into the film material. The ZrN film grown with nitrogen partial pressure at 17% of total pressure exhibits a stoichiometric composition, which shows the mellow gold color. The under-stoichiometric ZrN film exhibits in the color as silvery film and the over-stoichiometric ZrN film (N-rich film) exhibits in the color of red or brown gold [9], [10]. This is the same appearance as TiN material [6]. Thus, the nitrogen partial pressure in the process window for stoichiometric composition is in the range between 17-18% of the total pressure, which is considered narrow.

Table 1. The deposition rate, chemical composition and color of the ZrN films as a function of nitrogen partial pressure

| N <sub>2</sub> (%) | Deposition rate (nm/min) | Zr <sub>x</sub> N <sub>y</sub>     | Color      |
|--------------------|--------------------------|------------------------------------|------------|
| 14                 | 24.01                    | Zr <sub>1.7</sub> N <sub>0.3</sub> | silvery    |
| 17                 | 17.65                    | Zr <sub>1.1</sub> N <sub>0.9</sub> | golden     |
| 20                 | 10.19                    | Zr <sub>0.7</sub> N <sub>1.3</sub> | red golden |

Figure 1 shows the x-ray diffractograms of the ZrN thin films grown at different nitrogen partial pressures. For ZrN film grown at nitrogen partial pressure at 14%, the ZrN film consists of 2 main textures, the (111) and (220). As nitrogen partial pressures increased up to 17% of total pressure, the ZrN film exhibited in the (111), (200), (220) and (311). However, at nitrogen partial pressures at 20%, the ZrN (200) and (311) disappeared. Note that, for all the specimens, the (111) is still a preferred orientation for all nitrogen partial pressures.

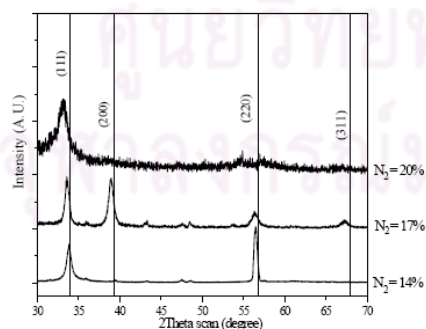


Figure 1 The X-ray diffraction patterns of the ZrN films with different nitrogen partial pressures

#### 3.2 Substrate Bias Voltage

With the optimum growth condition that gave a stoichiometric ZrN material at the nitrogen partial pressure at 17% of total pressure. The substrate negative bias voltage was applied to substrate from 0 V to 100 V to investigate the effect of ion bombardment during thin film growth. Prior before this work, the plasma potential was determine to be at 8 V, which obtained from the plasma characterization via Langmuir's probe. This can use in the calculation of the maximum kinetic energy of the bombarded ions. The elemental compositions of the ZrN films which are deposited at the nitrogen partial pressure 17% of total pressure with different the energies of assisted ions were again investigated and shown in table 2. The stoichiometry of the specimens is slightly changes when the substrate bias voltage was applied. The concentration of Zr in the ZrN films range form 48.48% to 51.53%, which still close to the stoichiometric form.

Table 2. The chemical composition of ZrN films grown at the nitrogen partial pressure is 17% of total pressure with different the energies of ions

| E <sub>i</sub> (eV) | Zr (at. %) | N <sub>2</sub> (at. %) | Zr <sub>x</sub> N <sub>y</sub>     |
|---------------------|------------|------------------------|------------------------------------|
| 8                   | 51.09      | 48.91                  | Zr <sub>1.1</sub> N <sub>0.9</sub> |
| 38                  | 51.53      | 48.47                  | Zr <sub>1.1</sub> N <sub>0.9</sub> |
| 58                  | 49.31      | 50.69                  | Zr <sub>0.9</sub> N <sub>1.1</sub> |
| 83                  | 48.48      | 51.52                  | Zr <sub>0.9</sub> N <sub>1.1</sub> |
| 108                 | 49.35      | 50.65                  | Zr <sub>0.9</sub> N <sub>1.1</sub> |

The comparison x-ray diffractograms of the ZrN films grown at the nitrogen partial pressure is 17% of total pressure with different the energies of assisted ions is shown in figure 2. The ZrN films still exhibited face center cubic phase and in the textures of (111), (200), (220) and (311) with substrate bias voltage is applied. However peak (311) slightly disappears as high energy of ions. The (111), (200), (220) and (311) correspond to the 2 theta at 33.9°, 39.3°, 56.8° and 67.9° respectively. The (111) peak is remain a preferred orientation for all the growths. However, at energy of ions is 38 eV results in the most development of (220) orientation from ion-assisted growth.

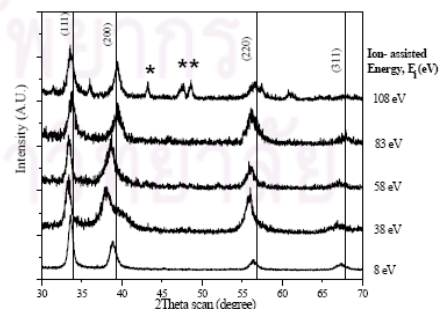


Figure 2 The X-ray diffraction patterns of the ZrN films grown at the nitrogen partial pressure is 17% of total pressure with different the energies of ions [\*represent substrate holder]

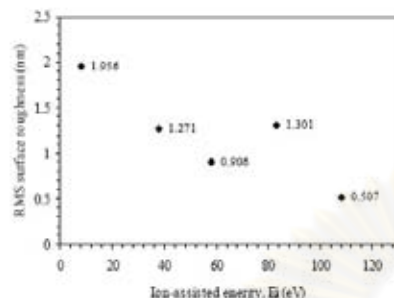


Figure 3 RMS surface roughness of the ZrN films grown at the nitrogen partial pressure is 17% of total pressure with different the energies of ions

From AFM measurements, the maximum root-mean-square roughness (RMS) is at 1.956 nm for the ZrN film grown with assisted-ions at energy of about 8 eV and decreases down to 0.507 nm for the ZrN film grown with ion energy at 108 eV, as illustrated in figure 3. The root-mean-square surface roughness tends to decrease as high substrate bias voltage is applied, thus high energy impact ions. This is due to at high substrate bias voltage, ions which are accelerated by electric field toward the substrate have a large energy induced an increasing in surface mobility of adatoms and help these adatoms move on surface to find the equilibrium lattice site. This results in a suppression of the 3-D island growth mechanism at low growth temperature regime [11], [12].



Figure 4 The AFM images of ZrN films deposited at ion energy of 0 eV (a), 38 eV (b), 58 eV (c), 83 eV (d), and 108 eV (e). (Data scale 30 nm)

The AFM images of ZrN films deposited at the energy of ions of 8 eV (a), 38 eV (b), 58 eV (c), 83 eV (d), and 108 eV (e) are also shown in figure 4. Thus that, the preferred surface morphology of ZrN films depends on the energy of ions which can be controlled.

For mechanical properties, the CSMT<sup>TM</sup> nanoindenter is used to determine the hardness of the ZrN films. A Berkovich diamond indenter tip is used with maximum indenter depth penetration was kept less than 10% of the film thickness. The maximum value of hardness is at 38.69 GPa for the film grown with the energy of ions of 38 eV. Compare to the film grown at normal condition, without ion assistance, the use of low-energy ion-assisted growth of ZrN can improve the hardness of the material up about 45%, which mean longer life-time use for the coated tools. At low substrate bias voltage, the ions near the substrate move to bombard the surface films and induce an increasing of the density of the films by an increasing of the surface diffusion [11]. For higher ion energies ( $E_i > 38\text{eV}$ ), the ions which are accelerated toward the substrate have a larger kinetic energy and cause higher momentum impact on the on-growing films. This result is leading to re-sputtering the weakly bonded atoms which effects on the mechanical properties of the films, and also reduces the deposition rate [3]. However, these results in smoother surface of the films as indicated from the AFM results.

#### 4. CONCLUSION

The Zirconium nitride (ZrN) films were deposited on silicon (100) substrates by reactive dc magnetron sputtering. The results clearly show the effects of nitrogen partial pressures and energy of ion bombardment on the surface of on-growing films via substrate bias voltage, on properties of ZrN films. The ZrN film grown at nitrogen partial pressure is 17% of total pressure gave stoichiometric composition film, which has a mellow gold color. The deposition rate decreases with nitrogen partial pressure increase due to the target nitriding effects where the sputtering yield for nitride is much smaller than the metal. The ZrN (200) texture which is the most stable and the hardest texture can be obtained with substrate bias voltage is applied where the nitrogen partial pressure is 17% of total pressure. The root-mean-square roughness tends to decrease as high substrate bias voltage is applied. The maximum value of hardness is 38.69 GPa with the energy of ions is 38 eV.

#### ACKNOWLEDGMENT

The authors would like to thank Department of Physics, Faculty of Science, Chulalongkorn University. This work has been supported by The 90th Anniversary of Chulalongkorn University Fund (Ratchadaphiseksomphot Endowment Fund).

#### REFERENCES

- [1] D. Pilloud, J.F. Pierson, A. Cavaleiro and M.C. Marco de Lucas. 2005. Effect of germanium addition on the properties of reactively sputtered ZrN films. *Thin Solid Films*. 492: 180-186.

- [2] Wen-Jun Chou, Ge-Ping Yu and Jia-Hong Huang. 2002. Bias effect of ion-plated zirconium nitride film on Si (100). *Thin Solid Films*, 405:162-169.
- [3] D. Pilloud, A.S. Dehlinger, J.F. Pierson, A. Roman and L. Pichon. 2003. Reactively sputtered zirconium nitride coatings: structural, mechanical, optical and electrical characteristics. *Surf. Coat. Technol.* 174-175: 338-344.
- [4] Jia-Hong Huang, Chi-Hsin Ho and Ge-Ping Yu. 2007. Effect of nitrogen flow rate on the structure and mechanical properties of ZrN thin films on Si (1 0 0) and stainless steel substrates. *Mater. Chem. Phys.* 102: 31-38.
- [5] D.F. Arias, Y.C. Arango and A. Devia. 2006. Study of TiN and ZrN thin films grown by cathodic arc technique. *Appl. Surf. Sci.* 253: 1683-1690.
- [6] M. Nose, M. Zhou, E. Honbo, M. Yokota and S. Saji. 2001. Colorimetric properties of ZrN and TiN coatings prepared by DC reactive sputtering. *Surf. Coat. Technol.* 142-144: 211-217.
- [7] Henry J. Ramos and Nicomedes B. Valmorira. 2004. Thin film deposition of ZrN using plasma sputter type negative ion source. *Vacuum*. 73: 549-554.
- [8] C.-S. Shin, D. Gall, Y.-W. Kim, N. Hellgren, I. Petrov and J. E. Greene. (2002). Development of preferred orientation in polycrystalline NaCl-structure  $\delta$ -TaN layers grown by reactive magnetron sputtering: role of low-energy ion/surface interactions. *J. Appl. Phys.* 92: 5084.
- [9] Chuan-Pu Liu and Heng-Ghieh Yang. 2003. Systematic study of the evolution of texture and electrical properties of ZrN<sub>x</sub> thin films by reactive DC magnetron sputtering. *Thin Solid Films* 444: 111-119.
- [10] Zhang Zhiguo, Liu Tianwei, Xu Jun, Deng Xinlu and Dong Chuang. 2006. N-rich Zr-N films deposited by unbalanced magnetron sputtering enhanced with a highly reactive MW-ECR plasma. *Surf. Coat. Technol.* 200: 4918-4922.
- [11] E.W. Niu, L. Li, G.H. Lv, H. Chen, W.R. Feng, S.H. Fan, S.Z. Yang and X.Z. Yang. 2007. Influence of substrate bias on the structure and properties of ZrN films deposited by cathodic vacuum arc. *Mater. Sci. Eng. A* 460-461: 135-139.
- [12] J.-H. Huang, K.-W. Lau and G.-P. Yu. 2005. Effect of nitrogen flow rate on structure and properties of nanocrystalline TiN thin films produced by unbalanced magnetron sputtering. *Surf. Coat. Technol.* 191: 17-24.

ศูนย์วิจัยทรัพยากร  
จุฬาลงกรณ์มหาวิทยาลัย

## Vitae

Miss Jirawan Saenton was born on October 27, 1983 in Phetchaboon, Thailand. She received her bachelor degree of Science in Physics from Naresuan University in 2006, and continued her Master's study at Chulalongkorn University in 2006.



ศูนย์วิจัยทรัพยากร  
จุฬาลงกรณ์มหาวิทยาลัย